NRL MEMORANDUM REPORT NO. 6894

MODELING OF DYNAMIC BIPOLAR PLASMA SHEATHS

J.M. Grossmann, S.B. Swanekamp, and P.F. Ottinger

Plasma Physics Division
Naval Research Laboratory
Washington, D.C. 20375-5000

August 20, 1991

REPORT DOCUMENTATION PAGE

Form Approved
OMB No 0704-0188

1. AGENCY USE ONLY (Leave blank)	2. REPORT DATE	3. REPORT TYPE AND DATES COVERED
	20 August 1991	Interim 10/1/90 - 9/30/91

4. TITLE AND SUBTITLE

"MODELING OF DYNAMIC BIPOLAR PLASMA SHEATHS"

5. FUNDING NUMBERS

47-3209-0-1

6. AUTHOR(S)

J.M. Grossmann
S.B. Swanekamp
P.F. Ottinger

7. PERFORMING ORGANIZATION NAME(S) AND ADDRESS(ES)

Code 4770
Plasma Physics Division
Naval Research Laboratory
Washington, DC 20375-5000

8. PERFORMING ORGANIZATION REPORT NUMBER

NRL Memorandum Report No. 6894

9. SPONSORING/MONITORING AGENCY NAME(S) AND ADDRESS(ES)

Office of Naval Research
800 N. Quincy Street
Arlington, VA 22217-5000

10. SPONSORING/MONITORING AGENCY REPORT NUMBER

11. SUPPLEMENTARY NOTES

This is an extended version of a paper already published in Physics of Fluids B (NRL 4770-180 dtd 6/13/91; NRL/JO-4770-180-91-0038/1-1221-1650).

12a. DISTRIBUTION/AVAILABILITY STATEMENT

Approved for public release, distribution is unlimited.

12b. DISTRIBUTION CODE

13. ABSTRACT (Maximum 200 words)

The behavior of a one dimensional plasma sheath is described in regimes where the sheath is not in equilibrium because it carries current densities that are either time dependent, or larger than the bipolar Child-Langmuir level determined from the injected ion flux. Earlier models of dynamic bipolar sheaths assumed that ions and electrons evolve in a series of quasi-equilibria. In addition, sheath growth was described by the equation $Zen_o x_s = |j_i| - Zen_o u_o$, where x_s is the velocity of the sheath edge, j_i is the ion current density, $n_o u_o$ is the injected ion flux density, and Ze is the ion charge. In this paper, a generalization of the bipolar electron-to-ion current density ratio formula is derived to study regimes where ions are not in equilibrium. A generalization of the above sheath growth equation is also developed which is consistent with the ion continuity equation and which reveals new physics of sheath behavior associated with the emitted electrons and their evolution. Based on these findings, two new models of dynamic bipolar sheaths are developed. Larger sheath sizes and potentials than those of earlier models are found. In certain regimes, explosive sheath growth is predicted.

14. SUBJECT TERMS

Plasma Sheaths
Inductive Storage
Diode Physics

15. NUMBER OF PAGES

63

16. PRICE CODE

17. SECURITY CLASSIFICATION OF REPORT	18. SECURITY CLASSIFICATION OF THIS PAGE	19. SECURITY CLASSIFICATION OF ABSTRACT	20. LIMITATION OF ABSTRACT
UNCLASSIFIED	UNCLASSIFIED	UNCLASSIFIED	Same as Report

GENERAL INSTRUCTIONS FOR COMPLETING SF 298

The Report Documentation Page (RDP) is used in announcing and cataloging reports. It is important that this information be consistent with the rest of the report, particularly the cover and title page. Instructions for filling in each block of the form follow. It is important to **stay within the lines to meet optical scanning requirements.**

Block 1. Agency Use Only (Leave Blank)

Block 2. Report Date. Full publication date including day, month, and year, if available (e.g. 1 Jan 88). Must cite at least the year.

Block 3. Type of Report and Dates Covered. State whether report is interim, final, etc. If applicable, enter inclusive report dates (e.g. 10 Jun 87 - 30 Jun 88).

Block 4. Title and Subtitle. A title is taken from the part of the report that provides the most meaningful and complete information. When a report is prepared in more than one volume, repeat the primary title, add volume number, and include subtitle for the specific volume. On classified documents enter the title classification in parentheses.

Block 5. Funding Numbers. To include contract and grant numbers; may include program element number(s), project number(s), task number(s), and work unit number(s). Use the following labels:

C	- Contract	**PR**	- Project
G	- Grant	**TA**	- Task
PE	- Program Element	**WU**	- Work Unit Accession No.

Block 6. Author(s). Name(s) of person(s) responsible for writing the report, performing the research, or credited with the content of the report. If editor or compiler, this should follow the name(s).

Block 7. Performing Organization Name(s) and Address(es). Self-explanatory.

Block 8. Performing Organization Report Number. Enter the unique alphanumeric report number(s) assigned by the organization performing the report.

Block 9. Sponsoring/Monitoring Agency Names(s) and Address(es). Self-explanatory.

Block 10. Sponsoring/Monitoring Agency. Report Number. (If known)

Block 11. Supplementary Notes. Enter information not included elsewhere such as: Prepared in cooperation with...; Trans. of ..., To be published in .... When a report is revised, include a statement whether the new report supersedes or supplements the older report.

Block 12a. Distribution/Availablity Statement. Denote public availability or limitation. Cite any availability to the public. Enter additional limitations or special markings in all capitals (e.g. NOFORN, REL, ITAR)

DOD	- See DoDD 5230.24, "Distribution Statements on Technical Documents."
DOE	- See authorities
NASA	- See Handbook NHB 2200.2.
NTIS	- Leave blank.

Block 12b. Distribution Code.

DOD	- DOD - Leave blank
DOE	- DOE - Enter DOE distribution categories from the Standard Distribution for Unclassified Scientific and Technical Reports
NASA	- NASA - Leave blank
NTIS	- NTIS - Leave blank.

Block 13. Abstract. Include a brief (Maximum 200 words) factual summary of the most significant information contained in the report.

Block 14. Subject Terms. Keywords or phrases identifying major subjects in the report.

Block 15. Number of Pages. Enter the total number of pages.

Block 16. Price Code. Enter appropriate price code (NTIS only).

Blocks 17. - 19. Security Classifications. Self-explanatory. Enter U.S. Security Classification in accordance with U.S. Security Regulations (i.e., UNCLASSIFIED). If form contains classified information, stamp classification on the top and bottom of the page.

Block 20. Limitation of Abstract. This block must be completed to assign a limitation to the abstract. Enter either UL (unlimited) or SAR (same as report). An entry in this block is necessary if the abstract is to be limited. If blank, the abstract is assumed to be unlimited.

NRL Memorandum Report No. 6894

MODELING OF DYNAMIC BIPOLAR PLASMA SHEATHS

J.M. Grossmann, S.B. Swanekamp, and P.F. Ottinger

Table of Contents

Modeling of Dynamic Bipolar Plasma Sheaths

J.M. Grossmann, S.B. Swanekamp*, and P.F. Ottinger

Abstract

The behavior of a one dimensional plasma sheath is described in regimes where the sheath is not in equilibrium because it carries current densities that are either time dependent, or larger than the bipolar Child-Langmuir level determined from the injected ion flux. Earlier models of dynamic bipolar sheaths assumed that ions and electrons evolve in a series of quasi-equilibria. In addition, sheath growth was described by the equation $Zen_o\dot{x}_s = |j_i| - Zen_o u_o$, where $\dot{x}_s$ is the velocity of the sheath edge, j_i is the ion current density, $n_o u_o$ is the injected ion flux density, and Ze is the ion charge. In this paper, a generalization of the bipolar electron-to-ion current density ratio formula is derived to study regimes where ions are not in equilibrium. A generalization of the above sheath growth equation is also developed which is consistent with the ion continuity equation and which reveals new physics of sheath behavior associated with the emitted electrons and their evolution. Based on these findings, two new models of dynamic bipolar sheaths are developed. Larger sheath sizes and potentials than those of earlier models are found. In certain regimes, explosive sheath growth is predicted.

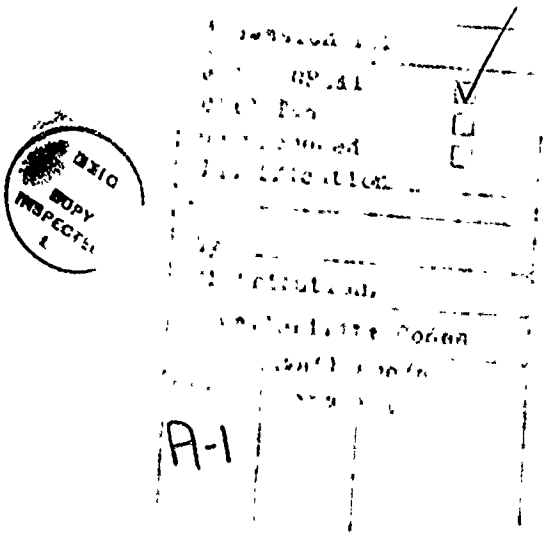

*NRL-NRC Postdoctoral Associate

I. Introduction

A plasma sheath is a transition region between a charge neutral plasma and a physical boundary where local charge neutrality no longer applies. These sheaths develop in any device where plasma is in contact with physical boundaries. As a result, the equilibrium properties of these sheaths have been studied thoroughly and are well understood. Examples of equilibrium sheaths include the Bohm sheath[1] and space charge limited flow[2].

Less well understood is the dynamic behavior of plasma sheaths in response to externally applied voltages or currents. Dynamic plasma sheaths have been studied for a wide variety of applications. These applications include plasma probes[3], vacuum discharge tubes[4,5], fusion reactors[6,7], rf plasma sources for thin-film fabrication technology[8], high voltage power systems for space applications[9], and pulsed power applications of plasma filled diodes (PFD)[10] and plasma erosion opening switches (PEOS)[11]. Motivation for the present work is provided by the PEOS and the PFD which are projected to be key components of inductive storage pulsed power systems.

An early reference to dynamic *ion* sheaths is Koch[12] who proposed that a dynamic cathode sheath develops in response to an external voltage. In this model the time rate of change of the sheath size is proportional to the difference between the ion current demanded by the Child-Langmuir equation[13] and the ion current available from the plasma. A rigorous proof of this model for ion sheaths was provided by Sander[4] who showed that the model is valid in the limit that the sheath growth is slow enough for the ions to respond. These ideas were expanded upon by Andrews and Varey[5] and by Widner, Alexeff, Jones, and Lonngren[14] to consider situations for which sheath dynamics occur on time scales faster than the ions can respond. Since the applied electric field was too low to stimulate explosive electron emission ($E<100$ kV/cm^2) in these experiments,

none of these early models considered electron emission into the sheath from the cathode. In the PEOS and PFD, however, field strengths in the sheath can be sufficient to achieve space-charge limited emission of electrons from the cathode. The first reference to dynamic *bipolar* sheaths which accounts for emitted electrons as well as ions is the paper by Miller, Poukey, and Wright[10]. In this model, the ion current density in Koch's ion sheath model is replaced with a bipolar flow model. This sheath growth model was later modified by Mendel and Goldstein to include relativistic effects[15]. Although these models have provided qualitative agreement with experiments in certain regimes, a rigorous proof of these formulas for dynamic bipolar sheaths has not been found in the literature. The development of such a theory is the intent of this paper.

The problem treated in this paper describes a dynamic bipolar sheath which forms at a one dimensional planar emitting electrode immersed in a fully ionized plasma. For simplicity, the plasma is assumed to have a uniform ion density, n_o, and an initial flow velocity, $-u_o$, where negative velocity signifies motion toward the cathode. High electron currents can produce a self-magnetic field that causes bending of the beam electron trajectories making the current flow pattern two dimensional. In the present work it is assumed that the self-magnetic field does not cause excessive bending of the electron orbits so that a one dimensional treatment is adequate. Physically, this might correspond to a situation in which beam currents are smaller than the critical current for beam pinching or magnetic insulation[16], or an external magnetic field is present to inhibit transverse beam motion.

A schematic of the one dimensional dynamic plasma sheath is shown in Fig. 1. The bipolar sheath is one in which electrons emitted from the cathode and ions drawn from the plasma are accelerated in the large sheath electric fields. It is further assumed that the voltage drop across the sheath is large compared with the plasma electron temperature, so that a sharp boundary exists between the neutral plasma, where electric

fields are small, and the non-neutral sheath region where large accelerating fields are present. Motion of the sheath/plasma boundary is provided by the acceleration of plasma electrons toward the anode. This acceleration is produced by an electric field which develops at the sheath edge either when current from the external circuit exceeds that which can be supported by the equilibrium bipolar sheath or when the current increases in time. As a result, plasma electrons leave the region of space near the sheath edge and redistribute themselves in the plasma to shield the sheath electric field from the bulk plasma. This process continues until the electric field at the newly formed sheath/plasma boundary is zero. Therefore, the net result of the plasma electron motion is to provide an additional ion flux into the sheath by uncovering ions as the sheath/plasma boundary recedes. These ions provide the additional positive charge required to ensure that the net sheath charge is zero so that the electric field vanishes at the sheath/plasma boundary. As an additional assumption, electron emission at the cathode is assumed to be space charge limited so that the electric field vanishes there as well.

In this paper, *plasma* electron dynamics are treated by a sequence of quasi-equilibrium states characterized by a density which is uniform inside the plasma and zero in the sheath. This uniform plasma electron density continually adjusts itself to maintain charge neutrality as beam electrons enter the plasma. Therefore, it is assumed that the net charge density from plasma ions, plasma electrons, and beam electrons is zero inside the plasma. Outside the scope of this paper is the mechanism by which this neutrality is maintained. Beam electrons, which are accelerated across the entire sheath rather than just near the sheath edge, generally obtain much higher velocities than the slower plasma electrons. The detailed interactions between beam electrons and plasma electrons, such as streaming instabilities are ignored in the present analysis, but have been treated elsewhere[17]. Therefore, the treatment of plasma electrons is adequate when sheath

dynamics occur on a time scale slow enough for plasma electrons to equilibrate and when beam-plasma interactions are weak.

Before presenting a detailed analysis of the dynamic plasma sheath, limitations of previous models are illustrated by examining a model which was used to describe PFD experiments[10]. In this treatment, charged particle flow in the sheath was modeled by the non-relativistic Child-Langmuir bipolar space-charge limited formulas

$$|j_b| = 1.86(4\varepsilon_o / 9)(2e / m_e)^{1/2} V_s^{3/2} / x_s^2 , \quad (1)$$

$$|j_i| = (Zm_e / m_i)^{1/2} |j_b| , \quad (2)$$

where j_i and j_b are the ion and beam electron current densities, x_s is the position of the sheath/plasma boundary, V_s is the potential drop across the sheath, Ze is the ion charge state, m_i and m_e are the ion and electron masses, and ε_o is the permittivity of free space in MKS units. Throughout this paper the subscripts i, b, and e will refer to ions, emitted beam electrons, and plasma electrons respectively. In Eqs. (1) and (2), absolute value signs have been used for the current densities since they are negative in the coordinate system depicted in Fig. 1. Strictly speaking, Eqs. (1) and (2) describe equilibrium ion and electron flow in a static sheath and are based on the assumptions of energy conservation and uniform current density across the sheath for both species. These equations can also be used to describe non-equilibrium sheaths as a sequence of quasi-steady states provided changes in the sheath electric field are slow enough for both ions and electrons to adjust.

As an illustration of the limitations of Eqs. (1) and (2), consider a dynamic sheath in which variations in the electric field occur on a time scale faster than the ions can respond. This situation can arise when the ion mass is very large or a large potential suddenly appears across the sheath causing the plasma electrons to quickly recede out of

the sheath. In either case, the assumptions of ion energy conservation and uniform ion current density do not apply. Therefore, the ion charge density can be substantially different from that predicted by the Child-Langmuir equations. In fact, if changes in the sheath electric field occur so fast that ions do not move appreciably, a uniform distribution of ion charge is more appropriate. The uniform ion density case has been referred to as the ion matrix limit in the literature on ion sheaths[5].

If τ_i and τ_e are the ion and electron equilibration times, and τ_s is the time scale for changes in the sheath electric field, then the dynamic behavior of bipolar sheaths can be divided into three different regimes: a slow regime characterized by $\tau_e << \tau_i << \tau_s$ where the assumptions of energy conservation and uniform current density are valid for both species and a bipolar model is appropriate, a moderately fast regime characterized by $\tau_e << \tau_s << \tau_i$ where the assumptions of energy conservation and uniform current density are appropriate for electrons but not for ions, and a fast regime characterized by $\tau_s << \tau_e << \tau_i$ where the assumptions of energy conservation and uniform current density are violated for both ions and electrons. Since electron dynamics are treated by a sequence of quasi-steady states, the models developed in this paper do not adequately describe sheath dynamics in the fast regime. This is not considered too restrictive for the purposes of this work since such fast time scales are not expected in most experiments of interest. However, with the PEOS and PFD it is possible for sheath fields to change on a time scale comparable with the ion time scale. In this paper a model is developed which extends previous treatments of dynamic bipolar sheaths to include the situation where sheath dynamics evolves fast on the ion time scale but slow on the electron time scale.

Returning to the examination of dynamic bipolar sheath models, the sheath opening equation used in previous models[10,15] was given as

$$|j_i| = Zen_o u_o + Zen_o \dot{x}_s , \tag{3}$$

where $\dot{x}_s$ is the velocity of the sheath edge. In Sec. II of this paper an exact version of Eq. (3) for dynamic bipolar sheaths is derived. In contrast to Eq. (3), the exact version fully obeys the ion continuity equation, and contains two correction terms arising from emitted electrons that are of importance in regimes of practical interest.

In this paper, a one-dimensional analytical treatment and numerical simulations of dynamic bipolar sheaths are presented. This new analysis includes a treatment of ion dynamics (non-equilibrium effects), electron emission and charge accumulation in the sheath, relativistic effects, and an initial ion injection velocity. In Sec. II, an equation describing the motion of the sheath/plasma boundary is presented. In Sec. III, an ion hydrodynamic approach is used to assess the role of ion dynamics on plasma sheaths and to develop a generalization of Eq. (2). In Sec. IV, complexities associated with Eq. (1) are discussed. Based on these discussions, an improved analytic model for sheath growth is developed in Sec. V. Although this analytic model is an improvement over previous models in its more accurate treatment of electron charge accumulation in the sheath, it is not adequate in regimes where ion dynamics are important because it treats ions by a sequence of quasi-steady states. A numerical model of the dynamic plasma sheath based on the particle-in-cell technique (PIC) is developed in Sec. VI. This numerical method features a PIC treatment of ions coupled with a quasi-steady-state treatment of electrons. In addition to including the new effects introduced in Secs. II - IV, the numerical model resolves ion dynamics and fully conforms to the ion continuity equation. The results of the models of Secs. V and VI are presented in Sec. VII and compared with ones used by previous authors. This comparison explicitly shows the limitations of models that neglect the emitted electron charge density and its evolution. It also points out the role of ion non-equilibrium effects and demonstrates regimes of interest where analytic models do not provide an adequate description of dynamic plasma sheaths. Finally, in Sec. VIII,

important conclusions of the present work are stressed and suggestions for future work are discussed.

II. An Equation for Dynamic Bipolar Sheath Growth

In this section an exact equation which governs the sheath size in one dimensional dynamic bipolar sheaths is presented. The equation for sheath growth can be derived from the continuity equation which is given by

$$\frac{\partial \rho}{\partial t} + \frac{\partial j}{\partial x} = 0 , \tag{4}$$

and Gauss's law,

$$\varepsilon_o \frac{\partial E}{\partial x} = \rho_i + \rho_b \ , \tag{5}$$

where $\rho(x,t)=\rho_i(x,t)+\rho_b(x,t)$ and $j(x,t)=j_i(x,t)+j_b(x,t)$ are the total charge and current densities , and ρ_i and ρ_b are the ion and beam electron charge densities in the sheath. Since the sheath/plasma boundary is sharp, no plasma electrons are in the sheath so that j_e and ρ_e are both zero there. If Eq. (5) is differentiated with respect to time and Eq. (4) is used to eliminate $\partial \rho / \partial t$, one obtains

$$\frac{\partial}{\partial x}[\varepsilon_o \frac{\partial E}{\partial t} + j(x,t)] = 0 . \tag{6}$$

Therefore, the quantity in brackets is independent of the spatial coordinate and is uniform across the sheath. To fix the constant, the quantity inside the brackets is evaluated at the cathode (x=0) where the electric field is zero by virtue of space-charge limited electron emission. The result is

$$\varepsilon_o \frac{\partial E}{\partial t} + j(x,t) = j(0,t) , \tag{7}$$

where $j(0,t)=j_i(0,t)+j_b(0,t)$ is the total current density at the cathode supplied by an external circuit. This last equation states that at every point inside the sheath the displacement current and conduction current must combine to give the current supplied by the external source.

Since the plasma electrons shield the sheath field from the bulk plasma, the electric field at the sheath edge, $E(x_s,t)$, is zero for all time. Therefore, it is possible to write

$$\varepsilon_o \frac{dE(x_s,t)}{dt} = 0 . \tag{8}$$

To derive an equation for $\dot{x}_s$, the time derivative in the last equation is expanded into its convective form

$$\varepsilon_o \frac{\partial E(x_s,t)}{\partial t} + \varepsilon_o \frac{\partial E(x_s,t)}{\partial x_s} \dot{x}_s = 0 . \tag{9}$$

Using Gauss's law to eliminate the spatial derivative of the electric field, an expression for the displacement current is given by

$$\varepsilon_o \frac{\partial E(x_s,t)}{\partial t} = -\rho_s \dot{x}_s , \tag{10}$$

where $\rho_s=\rho_i(x_s,t)+\rho_b(x_s,t)$ is the net charge density just inside the sheath. Since the bulk plasma is assumed to be charge neutral, $\rho_i+\rho_b+\rho_e=0$ inside the plasma. This assumption implies that the bulk plasma is field free, so that beam electrons stream freely through the plasma. Therefore, the beam density inside the plasma does not change from its value at the sheath/plasma boundary and the uniform plasma electron charge density is given by

$$\rho_e = -\rho_s . \tag{11}$$

Equations (10) and (11) show that the source of the non-equilibrium electric field at the sheath/plasma boundary is the motion of the plasma electrons.

If Eq. (7) is used to eliminate the dispiacement current, then Eq. (10) becomes

$$j_i(0,t) = j_i(x_s,t) - [\rho_i(x_s,t) + \rho_b(x_s,t)]\dot{x}_s + j_b(x_s,t) - j_b(0,t)\,, \tag{12}$$

where the ion and electron beam contributions to the total charge and current density have been separated. From the continuity equation for electrons, the difference between the electron current density at the sheath edge and the cathode can be expressed as

$$\Delta j_b \equiv j_b(x_s,t) - j_b(0,t) = -\int_0^{x_s} \frac{\partial \rho_b}{\partial t} dx\,. \tag{13}$$

Substituting this result into Eq. (12) and using the known plasma conditions at the sheath edge ($\rho_i(x_s,t) = Zen_o$, $j_i(x_s,t) = -Zen_o u_o$) gives

$$\left|j_i(0,t)\right| = Zen_o u_o + Zen_o\dot{x}_s + \rho_b(x_s,t)\dot{x}_s + \int_0^{x_s} \frac{\partial \rho_b}{\partial t} dx\,, \tag{14}$$

where $\left|j_i(0,t)\right| = -j_i(0,t)$ has been used since $j_i(0,t)$ is negative. An alternate form of Eq. (14) can be derived by noting that the last two terms form an exact time differential giving the following more compact expression

$$\left|j_i(0,t)\right| = Zen_o u_o + Zen_o\dot{x}_s + \frac{d}{dt}\int_0^{x_s} \rho_b(x,t)dx\,. \tag{15}$$

Equation (15) shows that sheath growth is affected not only by the difference between the ion current density at the two ends of the sheath, $\left|j_i(0,t)\right| - Zen_o u_o$, but also by the changing emitted electron charge as the sheath grows. Thus, even when the ion current density is uniform in the sheath, the sheath will still grow if the emitted electron charge in the sheath increases. A comparison of Eqs. (3) and (15) shows that previous gap opening formulas are recovered provided j_i in Eq. (3) is interpreted as the ion current density at the cathode and the time rate of change of the total emitted electron charge in

the sheath is ignored. Note that Eq. (15) can be also be derived directly from the ion continuity equation and by recognizing that Gauss's law implies that, when the electric field vanishes at both ends of the sheath, the net charge in the sheath is zero. Therefore, Eq. (15) can also be interpreted as a statement of ion continuity in the dynamic sheath.

When the electron current is increasing, the rate at which electron charge is supplied to the sheath is negative. Therefore, Eq. (15) shows that electron emission leads to sheath growth that is larger than that predicted by Eq. (3). As an illustration of the importance of the emitted electrons, consider a dynamic bipolar sheath in the ion matrix limit (i.e. $\tau_s << \tau_i$). In this case one expects the sheath electric field to have little affect on the ion trajectories so that the difference between the ion current density at the sheath edge and the cathode is small (i.e. $|j_i(0,t)| \cong Zen_o u_o$). If $\partial\rho_b / \partial t$ in Eq. (14) were set to zero, or if the rate of change of the total sheath electron charge in Eq. (15) were ignored, $\dot{x}_s$ would be incorrectly predicted to be zero. Thus, the inclusion of the evolution of the emitted electron charge in the sheath growth equation adds important new physics which has not been treated previously. Another new feature of these equations is the possibility of singular sheath growth because of cancellation of the ion and electron charge density at the sheath/plasma boundary. In Eq. (14), if $Zen_o u_o + \rho_b(x_s,t)$ approaches zero, $\dot{x}_s$ can become very large, provided the other terms in the equation do not also vanish. This singularity, as well as the importance of the last terms of Eqs. (14) and (15), will be discussed in more detail in Sec. VII.

III. A Generalized Current Density Relationship.

In the introduction, some of the main assumptions and limitations of previous dynamic sheath models have been described. In this section, a generalization of the Child-Langmuir current density ratio, Eq. (2), is derived for the case where ions are not in equilibrium. This generalization identifies regimes where ion inertia effects may be

important and is useful in interpreting the numerical results presented in Sec. VII. The important assumptions of this section include: energy conservation for beam electrons, that the electric field vanishes at both ends of the sheath, and that the electron beam current density is nearly uniform.

Non-equilibrium ion behavior in dynamic plasma sheaths can be described by the hydrodynamic equations

$$\frac{\partial \rho_i}{\partial t} + \frac{\partial j_i}{\partial x} = 0, \tag{16}$$

and,

$$\frac{\partial v_i}{\partial t} + v_i \frac{\partial v_i}{\partial x} = \frac{ZeE}{m_i} . \tag{17}$$

The electric field, E, is computed from Gauss's law, Eq. (5).

Since changes in the sheath electric field are assumed to occur slowly enough for electrons to equilibrate, beam electron dynamics can be treated by a sequence of quasi-steady states. In quasi-steady state, the momentum transfer equation for beam electrons implies their energy is conserved across the sheath. This condition is expressed as

$$\gamma(x,t) = 1 + \frac{e\phi(x,t)}{m_e c^2} , \tag{18}$$

where $\gamma(x,t)$ is the relativistic mass factor for the beam electrons, c is the speed of light, and $\phi(x,t)$ is the electric potential. When inductive fields due to rising sheath currents are negligible, the potential can be related to the electric field by

$$E = -\frac{\partial \phi}{\partial x} = -\frac{m_e c^2}{e} \frac{\partial \gamma}{\partial x} . \tag{19}$$

The electron charge density in the sheath can be expressed in terms of the beam current density and the relativistic mass factor as

$$\rho_b(x,t) = \frac{-|j_b(t)|}{v_b(x,t)} = \frac{-|j_b(t)|}{c}\frac{\gamma(x,t)}{\sqrt{\gamma^2(x,t)-1}} \quad , \tag{20}$$

where $v_b(x,t)$ is the beam electron fluid velocity. Both in earlier sheath models and in the work presented in this paper, this equation is used to estimate the emitted electron charge density in the sheath. In deriving Eq. (20), it has been assumed that the electron current density is spatially uniform, even though both the electron current density and the potential are allowed to vary in time so that, in general,

$$\frac{\partial \rho_b}{\partial t} = \frac{\partial}{\partial t}\left(\frac{-|j_b(t)|}{c}\frac{\gamma}{\sqrt{\gamma^2-1}}\right) = -\frac{\partial j_b}{\partial x} \neq 0 \quad . \tag{21}$$

Despite this inconsistency with the electron continuity equation, Eq. (20) is a good estimate of the electron charge density as long as the spatial non-uniformity of j_b dictated by Eq. (21) is small compared with j_b. This point reflects back to the sheath equations of Sec. II. There the term Δj_b of Eq. (13), and implicitly contained in Eq. (14), was introduced as an important contributor to the sheath opening equation in the ion matrix limit. Thus, spatial non-uniformities in j_b are assumed insignificant in estimating the electron charge density of Eq. (20), while they may contribute significantly to the sheath growth predicted by Eq. (14). This apparent contradiction is resolved by comparing $|\Delta j_b|$ with the other terms in the respective equations. In Eq. (14), $|\Delta j_b|$ should be compared with $|\Delta j_i| = |j_i(0,t) - Zen_o u_o|$, while in Eq. (20), it should be compared with $|j_b|$. Since $|j_b(t)|$ is usually much greater than $|\Delta j_i|$ (see Eq. (2)), $|\Delta j_b|$ can be important to sheath growth without significantly disturbing the density estimate.

The method used to develop a non-equilibrium, time dependent version of the Child-Langmuir current density ratio for dynamic bipolar sheaths is similar to one used by Kadish et. al[18], except that emitted electrons are included. The fundamental equation can be derived by multiplying Eq. (16) by v_i, Eq. (17) by ρ_i, and adding. The result is

$$\frac{\partial j_i}{\partial t}+\frac{\partial (j_i v_i)}{\partial x}=\frac{Ze}{m_i}\rho_i E\,. \tag{22}$$

If Gauss's law [Eq. (5)] is used to eliminate ρ_i,and j_b is assumed uniform, Eq. (22) can be written as

$$\frac{\partial j_i}{\partial t}+\frac{\partial}{\partial x}\left[j_i v_i-\frac{Ze}{2m_i}\varepsilon_o E^2+|j_b(t)|c\frac{Zm_e}{m_i}\left(\gamma^2-1\right)^{1/2}\right]=0\,, \tag{23}$$

where Eqs. (19) and (20) have been used to eliminate the product $\rho_b E$. Spatially integrating across the sheath and using the boundary conditions on the electric field, this last equation becomes

$$j_i(0,t)v_i(0,t)+j_i(x_s,t)u_o-|j_b(t)|c\frac{Zm_e}{m_i}\left(\gamma_o^2(t)-1\right)^{1/2}=\int_0^{x_s}\frac{\partial j_i}{\partial t}dx\,. \tag{24}$$

In Eq. (24), the additional boundary conditions of $v_i(x_s,t) = -u_o$, $\gamma(x=0,t) = 1$ and $\gamma(x_s,t) = \gamma_o(t) = 1+eV_s(t)/m_ec^2$ have been used. From Eq. (18) it is seen that the boundary conditions on γ are consistent with the boundary conditions on ϕ namely, $\phi(0,t)=0$ and $\phi(x_s,t)=V_s(t)$. The ion momentum transfer equation [Eq. (17)] can be used to eliminate the ion velocity at the cathode in Eq. (24). To do this, Eqs. (17) and (19) are combined to give

$$\frac{\partial (m_i v_i)}{\partial t}+\frac{\partial}{\partial x}\left[\frac{1}{2}m_i v_i^2+Zm_e c^2(\gamma-1)\right]=0\,. \tag{25}$$

Spatially integrating this last equation yields an expression for the ion velocity in the sheath,

$$v_i(x,t) = -c\left(\frac{2Zm_e}{m_i}\right)^{1/2}\left[\gamma_o + \gamma_F - \gamma\right]^{1/2}\left[1 + \frac{\int_x^{x_s}\frac{\partial(m_i v_i)}{\partial t}dx}{Zm_e c^2\left[\gamma_o + \gamma_F - \gamma\right]}\right]^{1/2}, \qquad (26)$$

where the parameter $\gamma_F \equiv m_i u_o^2/2Zm_e c^2$ has been introduced. Equation (24) and Eq.(26) evaluated at x = 0 describe a relationship between the electron and ion current densities in the sheath and the potential drop across the sheath, and may be viewed as the dynamic analog of Eq. (2). Given the importance of the term $j_i(0,t)$ in Eq. (14) for sheath opening, approximations to Eqs. (24) and (26) will be examined in the remainder of this section in order to understand their physical significance in the ion inertial regime.

In earlier models, energy conservation for the ions across the sheath was assumed. This amounts to the neglect of the term in Eq. (26) involving the integration compared with unity. When this assumption is valid, Eq. (26) becomes

$$v_i(x,t) \cong -c\left(\frac{2Zm_e}{m_i}\right)^{1/2}\left[\gamma_o(t) + \gamma_F - \gamma(x,t)\right]^{1/2}. \qquad (27)$$

As pointed out in the introduction, the assumption of energy conservation for ions across the sheath is questionable when sheath dynamics evolves on a time scale comparable with, or faster than, that on which ions can respond.

In order to investigate when ion inertia effects may be important, Eq. (24) is examined to determine the regime where the ion current density approaches the equilibrium bipolar result. In the process, an approximate form of Eq. (24) is derived. To do this, Eq. (26) is expanded to first order by assuming that the integral term is small

compared with unity. This estimate of the ion velocity is then substituted in Eq. (24) to give

$$j_i(0,t) \cong j_i^{BP}(t) - \frac{(m_i/2Zm_e)^{1/2}}{\left[(\gamma_o(t)+\gamma_F-1)^{1/2}-\gamma_F^{1/2}\right]}\frac{1}{c}\int_0^{x_s}\frac{\partial j_i}{\partial t}dx - \frac{\gamma_F^{1/2}[j_i(0,t)-j_i(x_s,t)]}{\left[(\gamma_o(t)+\gamma_F-1)^{1/2}-\gamma_F^{1/2}\right]}$$
$$- \frac{j_i(0,t)(m_i/2Zm_e)}{(\gamma_o(t)+\gamma_F-1)^{1/2}\left[(\gamma_o(t)+\gamma_F-1)^{1/2}-\gamma_F^{1/2}\right]}\frac{1}{c^2}\int_0^{x_s}\frac{\partial v_i}{\partial t}dx, \qquad (28)$$

where $j_i^{BP}(t)$ is the time-dependent Child-Langmuir bipolar space-charge limited current density defined by

$$j_i^{BP}(t) = -|j_b(t)|\left(\frac{Zm_e}{m_i}\right)^{1/2}\left(\frac{\gamma_o(t)+1}{2}\right)^{1/2}\frac{(\gamma_o(t)-1)^{1/2}}{\left[(\gamma_o(t)+\gamma_F-1)^{1/2}-\gamma_F^{1/2}\right]}. \qquad (29)$$

In steady state, Eq. (28) reduces to the equilibrium bipolar density formula [Eq. (29)] which is both relativistically correct and includes an initial ion injection velocity. Equation (29) is the quasi-static generalization of the bipolar current ratio and reduces to Eq. (2) in the limit as $\gamma \to 1$ and $u_o \to 0$. Equation (28) demonstrates that $j_i(0,t) \cong j_i^{BP}(t)$, provided that the sum of the last three terms on the right hand side is small compared with $j_i^{BP}(t)$. In the following paragraphs, first order corrections to each of the last three terms on the right hand side of Eq. (28) will be analyzed separately to examine the validity of the approximation $j_i(0,t) \cong j_i^{BP}(t)$.

To estimate the importance of the second term on the right of Eq. (28), assume that the ion current density is approximately uniform so that $j_i(x,t) \cong j_i^{BP}(t)$. In this case the spatial integration of that term can be approximated by

$$\int_0^{x_s}\frac{\partial j_i}{\partial t}dx \cong x_s\frac{dj_i^{BP}}{dt}. \qquad (30)$$

Using this approximation in Eq. (28), it is seen that the second term can be neglected when

$$\frac{1}{j_i^{BP}}\frac{dj_i^{BP}}{dt} << \tau_i^{-1} \cong \frac{c}{x_s}\left(\frac{2Zm_e}{m_i}\right)^{1/2}\left[(\gamma_o+\gamma_F-1)^{1/2}-\gamma_F^{1/2}\right]. \tag{31}$$

Therefore, the first conclusion to be made about ion dynamics in plasma sheaths is that the second term on the right of Eq. (28) is negligible as long as changes in the ion current density occur more slowly than τ_i. It can be shown from Eq. (27) that $\tau_i \cong x_s/|v_i(0,t)|$ when γ_F is small compared with (γ_o-1). Under this condition τ_i can be interpreted as a lower bound on the ion transit time, since $|v_i(0,t)|$ is the maximum speed of the accelerating ions.

Next, the importance of the third term on the right hand side of Eq. (28) is considered. This term can be ignored only when it is small compared with $j_i^{BP}(t)$, placing limitations on the degree of non-uniformity in the ion current density which can be tolerated before the approximation $j_i(0,t) \cong j_i^{BP}(t)$ breaks down. Using Eq. (15) from Sec. II, this limitation can be expressed as

$$\left(\frac{Zen_ou_o}{\left|j_i^{BP}(t)\right|}\right)\left[\frac{\dot{x}_s}{x_s}+\frac{1}{x_s}\frac{d}{dt}\int_0^{x_s}\frac{\rho_b(x,t)}{Zen_o}dx\right] << \tau_i^{-1}. \tag{32}$$

where τ_i is defined in Eq. (31). Therefore, the second conclusion to be made about ion dynamics in bipolar sheaths is that the third term in Eq. (28) is negligible when changes in either the sheath size or the amount of emitted electron space charge supplied to the sheath occur on a time scale which is slow compared with τ_i.

The importance of a non-equilibrium ion fluid velocity can be estimated from the relative size of the last term on the right hand side of Eq. (28) compared with $j_i^{BP}(t)$.

Using the ion conservation of energy equation, the last term of Eq. (28) can be ignored when

$$\frac{j_i(0,t)}{j_i^{BP}(t)}\left\{\frac{\int_0^{x_s}\frac{\partial}{\partial t}\left[\gamma_o(t)+\gamma_F-\gamma(x,t)\right]^{1/2}\frac{dx}{x_s}}{\left[\gamma_o(t)+\gamma_F-1\right]^{1/2}}\right\}<<\tau_i^{-1} \tag{33}$$

The left hand side of the last inequality is related to the time scale for changes in the potential distribution. Therefore, the third conclusion to be made about ion dynamics in bipolar sheaths is that the fourth term is negligible when changes in the potential distribution occur on a time scale which is slower than τ_i.

The results of this section show that, when τ_i is small compared with the time scale for changes in the system parameters, then the approximation $j_i(0,t) \cong j_i^{BP}(t)$ is good and ion inertia effects are not important. However, the converse is not necessarily true. Large values of τ_i do not necessarily mean that $j_i(0,t) \cong j_i^{BP}(t)$ is a bad approximation since cancellation between the terms in Eq. (29) can occur in some circumstances. In Sec. VII, examples of this cancellation will be shown. Despite these caveats, τ_i is often a good indicator of when the approximation $j_i(0,t) \cong j_i^{BP}(t)$ breaks down and ion inertia effects are important. This is expected because τ_i is related to the ion transit time. When the changes described in Eqs. (31)-(33) occur on a time scale comparable to or faster than τ_i, non-equilibrium ion behavior may have a significant effect on the evolution of dynamic bipolar sheaths. In this case, an accurate treatment of ion dynamics is needed.

IV. Child-Langmuir Equation for Dynamic Sheaths

In this brief section, some of the subtleties associated with calculating $\gamma(x,t)$ are discussed. Since γ is related to ϕ through Eq. (18), this is equivalent to solving the

relativistic version of Poisson's equation. The resulting solution, evaluated at x_s will provide the version of Eq. (1) that will be used in later sections. This new equation will be the equivalent of the Child-Langmuir equation for dynamic bipolar space charge limited flow. To calculate the potential, the electron and ion charge densities in the system must be determined. When the electrons can be assumed to evolve in a series of quasi-steady-states, Eq. (20) is a reasonable estimate for the electron density. Combining Eqs. (5), (19) and (20), an equation for $\gamma(x,t)$ can be written as

$$\frac{\partial^2 \gamma}{\partial x^2} = \left(\frac{e}{\varepsilon_o m_e c^3} \right) \left[\frac{\gamma |j_b(t)|}{(\gamma^2 - 1)^{1/2}} - c\rho_i(x,t) \right], \tag{34}$$

where the boundary conditions on $\gamma(x,t)$ are given in the text following Eq. (24). To ensure that the electric field vanish at both ends of the sheath, an additional requirement on Eq. (34) is that $\partial\gamma / \partial x$ be zero at the cathode and the sheath/plasma boundary.

Given $j_b(t)$, an expression for $\rho_i(x,t)$ must be given to completely determine $\gamma(x,t)$. In the limit of inertia-less ions (i.e. as $m_i \rightarrow 0$, or $\tau_i << \tau_s$), the ion current density is uniform except for a small region near the sheath/plasma boundary. If this region of non-equilibrium ion behavior is small compared with the sheath size, then $\rho_i(x,t)$ is well approximated by $j_i / v_i(x,t)$. Furthermore, in this case, energy conservation for ions is a good assumption, so that Eq. (27) can be used to express v_i as a function of $\gamma(x,t)$. This will be the approach taken in the next section. In the limit of infinitely massive ions (i.e. $m_i \rightarrow \infty$ or $\tau_i >> \tau_s$), the ion matrix model is appropriate with ρ_i = constant. In Sec. VI, the intent is to treat the dynamic regime between these two limits where it is difficult to write an analytic expression for ρ_i. In this regime where ion inertia effects are pronounced, a PIC treatment of the ions is a convenient method for computing ρ_i for use in the numerical solution of Eq. (34).

V. The Modified Bipolar Model

In Sec. II, an equation was developed relating the motion of the sheath/plasma boundary, the ion current density, and the time rate of change of the emitted electron charge in the sheath. The fundamental result of that section is given in Eq. (14). This equation illustrates the limitations of Eq. (3) and reveals new physics involving the role of emitted electrons in dynamic plasma sheaths. In Sec. III a more general version of Eq. (2), the bipolar current density ratio, was developed. The role of ion inertia was examined in detail and conditions on the validity of treating ion dynamics by a sequence of quasi-steady states were developed. The limitations of a quasi-steady state treatment of ion dynamics are summarized by the three inequalities given in Eqs. (31), (32), and (33). Several prescriptions for determining the ion charge density for dynamic sheaths was given in the last section. In this section ion dynamics is modeled by a sequence of quasi-steady-states without a priori justification.

First, the sheath opening formula, Eq. (2), is modified by including the second to last term of Eq. (14) and solving for $\dot{x}_s$ to yield,

$$\dot{x}_s = \frac{|j_i(0,t)| - Zen_o u_o}{Zen_o + \rho_b(x_s,t)}. \tag{35}$$

In Eq. (35), the Δj_b term of Eq. (14) has been assumed to be negligible compared with the remaining terms. In the examples studied in Sec. VII, this will shown to be a good approximation in certain cases, and a significant improvement over Eq. (2) in all cases. Note that Eq. (35) allows the possibility of singular sheath growth when $\rho_b = -Zen_o$, resulting in very rapid sheath growth. To obtain solutions to Eq. (35), an expression for $j_i(0,t)$ must be found. The modified bipolar model assumes that the ion current density is uniform and that ions have sufficient time to relax to equilibrium. Then in keeping with the steady-state limit of Eq. (28),

$$j_i(x,t) \cong j_i(0,t) \cong j_i^{BP}(t), \tag{36}$$

where $x < x_s$ and j_i^{BP} is given by Eq. (29).

To calculate j_i^{BP}, Eq.(34) must be solved for $\gamma_o(t)$ which, in turn, requires an expression for $\rho_i(x,t)$. In the present quasi-equilibrium ion model, ions obey energy conservation, so $\rho_i(x,t)$ can be written as

$$\rho_i(x,t) \cong \frac{\left|j_i^{BP}(t)\right|}{c} \frac{(m_i / 2Zm_e)^{1/2}}{[\gamma_o(t) + \gamma_F - \gamma(x,t)]^{1/2}}, \tag{37}$$

where γ_F is a parameter determined by the initial ion velocity and is defined after Eq. (26). The main assumptions built into Eq. (37) are conservation of ion energy and uniform ion current density in the sheath. These assumptions are not strictly correct since Eq. (26) explicitly shows that ion energy is not conserved when ion inertia effects are important, and Eq. (35) explicitly allows the ion current densities at the cathode and sheath/plasma boundary to be different in dynamic bipolar sheaths. One consequence of these assumptions is that Eq. (37) overestimates the ion charge density at the sheath/plasma boundary whenever $\left|j_i^{BP}(t)\right|$ exceeds the initial ion flux $Zen_o u_o$. In Sec. VII, it will be seen that $\left|j_i^{BP}(t)\right|$ is generally much larger than $Zen_o u_o$. For these reasons, Eq. (37) does not provide an accurate estimate of the ion charge density near the sheath/plasma boundary. However, when changes in the sheath parameters are reasonably slow compared with τ_i, non-equilibrium ion behavior can be confined to a small spatial region very close to the sheath/plasma boundary. In this case, Eq. (37) can still provide a reasonable estimate of the ion charge density over most of the sheath and hence produce a good estimate of $\gamma(x,t)$ when used in Eq. (34). This point will be illustrated when the results of this model are given in Sec. VII.

Substituting Eq. (37) into Eq. (34) and spatially integrating once, the differential equation for $\gamma(x,t)$ becomes

$$\frac{\partial\gamma}{\partial x}=\left(\frac{2e}{\varepsilon_o m_e c^3}\right)^{1/2}\left\{\left|j_b(t)\right|(\gamma^2-1)^{1/2}-\left|j_i^{BP}(t)\right|(2m_i/Zm_e)^{1/2}\right.$$
$$\left.\times\left[(\gamma_o(t)+\gamma_F-1)^{1/2}-(\gamma_o(t)+\gamma_F-\gamma)^{1/2}\right]\right\}^{1/2}, \qquad (38)$$

where the relationship between $j_b(t)$ and $j_i^{BP}(t)$ given by Eq. (29) ensures that the electric field vanishes at the sheath/plasma boundary. In general, Eq. (38) has no closed form solution but can be integrated numerically and iterated to find the solution which satisfies the boundary conditions on γ. The numerical solution of Eq. (38) together with Eqs. (18) and (29) provides a relationship between the voltage drop across the sheath and the electron current density and is the analog of Eq. (1).

In concluding this section, the equations analogous to Eqs. (1) - (3) used in the modified bipolar model are summarized. Equation (38), together with the its boundary conditions is the analog of Eq. (1). Equation (38) incorporates the added complexity of relativistic considerations and an initial ion velocity. The assumption in Eq. (36) that $j_i(0,t)\cong j_i^{BP}(t)$ is the relativistic version of the bipolar current density ratio given in Eq. (2) and is used in Eq. (37) to provide an estimate of the ion density. Motion of the sheath/plasma boundary is provided by Eq. (35) which is the analog of Eq. (3). Once $j_b(t)$ is specified, Eqs. (35), (36) and (38) can be solved as a sequence of quasi-steady states in much the same way as was done previously with Eqs. (1)-(3). In addition to the specification of plasma parameters, the main input to the modified bipolar model is $j_b(t)$. If the sheath is driven by an external circuit then, by assuming that current is continuous across the cathode surface, the time dependence of $j_b(t)$ can be determined directly from the current provided by the external circuit and the ion current density at the cathode. In

this model and the one of Sec. VI, the added complexity of a driving circuit is avoided by assuming a known time dependence for $j_b(t)$. This assumption is considered adequate for the purpose of demonstrating the role of electron and ion dynamics in non-equilibrium bipolar sheaths. The results of calculations using the modified bipolar sheath model are presented in Sec. VII together with the results of the numerical model described in the next section. It will be seen that despite the many questionable assumptions built into it, the model produces significantly better agreement with the results of the numerical model than earlier approaches.

VI. Dynamic Sheath Opening Based On Numerical Simulation

In previous sections, ion dynamics are treated by a sequence of quasi-steady-states. The numerical model for sheath opening, called PIC/CLO, calculates ion dynamics by the particle-in-cell method[19]. As with the analytic modeling, the plasma region outside the sheath between the sheath edge and the anode is not treated in any detail except as a source of ions as the plasma electrons recede. As the sheath grows, it is assumed that a uniform background of ion density is available to it at the sheath/plasma boundary. Beam electrons are assumed to evolve through a sequence of quasi-equilibrium states, so that Eq.(20) is used as an approximation for their charge density. In using this estimate for $\rho_b(x,t)$, the models used both in the past and in this paper assume electron energy conservation and uniform electron current density even though the electric field and electron charge density are time dependent. In order to estimate the errors associated with these assumptions, diagnostics were included in PIC/CLO to measure the degree to which electron continuity and energy conservation are violated. These errors are less than 1% in all but the most extreme case described in this paper, where it grows to about 6%.

The ion density in PIC/CLO is found by summing the charge contributions on the mesh of each of the particles using triangular shape factors. Equation (34) is integrated numerically to find γ using the boundary conditions that the electric field vanish at the cathode, and that $\gamma(x=0,t)=1$. The plasma/sheath boundary is defined by the position where the electric field returns to zero. Given $\gamma(x,t)$ everywhere in the sheath, the electric field is found from Eq. (19) and used to push each of the macroparticles in the ion equation of motion,

$$m_i \frac{dv_i}{dt} = ZeE(x,t). \tag{39}$$

The ion distribution is initially uniform, and all ions have an initial velocity $-u_o$. Only the ions in the sheath are accelerated according to Eq. (39), while ions outside of the sheath move ballistically with velocity $-u_o$ since E = 0 in the plasma. Input to PIC/CLO consists of the initial ion density and injection velocity, and the time dependent electron current density carried by the sheath. Output from PIC/CLO includes the evolving sheath size, and related time dependent quantities such as the sheath potential, the electron density at the sheath/plasma boundary, and the ion current density at the cathode. The numerical model presented here is similar to the one originally used by Sander[4] to examine ion dynamics in ion sheaths, except that electron emission is included. It improves on the modified bipolar sheath model described in Sec. V by including a more accurate treatment of ion dynamics and of the effect of the time-varying electron charge in the sheath. Except under extreme conditions, where numerical errors come into play, PIC/CLO obeys the full hydrodynamic relation, Eq. (24), and the sheath opening equation, Eq. (14).

VII. Results

In this section, the results of the computational model outlined in Sec. VI are compared with the analytic model described in Sec. V and with earlier treatments of sheath dynamics. Results are given for five cases summarized in Table I, and selected for their relevance to PFD and PEOS theory and experiment. In addition to displaying the characteristics of dynamic sheaths, results are chosen to demonstrate the points made in Secs. II-V such as: the accuracy of the modified bipolar approximation for the ion current density given in Eq. (36), the effect of ion inertia, and the importance of including the electron charge density terms in Eq. (14) to model sheath growth.

In all five cases the ion species used is doubly ionized carbon. The cases vary only in the initial plasma density, injection velocity, and rate of electron current density rise. As seen in Table I, two ion densities are used, 10^{12} cm^{-3}, and 10^{13} cm^{-3}. The injection velocity associated with all 10^{12} cm^{-3} cases is 10 cm/μs, while the injection velocity for all 10^{13} cm^{-3} cases is 1 cm/μs. These velocities were chosen so that the ion flux in all cases is identical, thus allowing fairer comparison between cases in which the driven electron current densities are the same, but the ion densities differ.

The simulations were all started with a small but non-zero initial beam current density, $j_o = -336$ A/cm^2. This corresponds to the simple bipolar value, Eq. (2), using the injected ion current density, $-Zen_ou_o = -3.2$ A/cm^2. In the examples shown here, the beam electron current density is assumed to rise linearly with time and take the form

$$j_b(t) = j_o + t\,\frac{dj_b}{dt}\,, \tag{40}$$

where dj_b/dt is the fixed rate of current density rise listed in Table I in each case. For the first two cases, a 10^{12} cm^{-3}, and 10^{13} cm^{-3} plasma is driven with an electron current density that rises at the rate of -0.1 kA/cm^2-ns. In the next two cases these same two densities are driven at the rate of -1 kA/cm^2-ns. In the fifth case, a 10^{12} cm^{-3} plasma is

driven at a rate of -4 kA/cm^2-ns. Except in cases 4 and 5, the simulations are run for a total of 10 ns. Cases 4 and 5 are stopped at earlier times to avoid errors associated with rapid sheath growth. In Table I, the stopping time in each case is shown in the row labelled t_o.

The first four problems were chosen for their relevance to plasma filled diode experiments, where a 5 cm radius diode might be expected to conduct a 1 MA pulse that rises in about 10 ns. However, because magnetic effects are neglected in this (one dimensional) treatment, the results presented here strictly apply when the critical current is not exceeded. When the critical current is exceeded, it is assumed that one-dimensional flow is maintained through the introduction of a strong external magnetic field in the direction of the electron flow. The fifth case examined in this paper is intended to show the extremes of behavior predicted in the present model. It is also in a regime relevant to 2 1/2 dimensional simulations of a short conduction time (50-100ns) PEOS. These simulations feature an intense current channel which migrates axially along the cathode, producing regions where the electron current density is largely normal to the cathode and rises rapidly to high values[20]. In these 2 1/2-D cylindrical simulations, radial beam current flow is maintained in the presence of a strong azimuthal magnetic field as a result of electrostatic fields transverse to the electron flow. These axial electric fields allow laminar ExB electron flow in the direction normal to the cathode.

In each of the five cases, the sheath size found in PIC/CLO is compared with earlier models and with the modified bipolar model presented in Sec. V. In order to understand the physical reasons for the differences between the models, analysis of the results will be given in terms of the ideas introduced in Secs. II-IV. It will be seen that the additional terms in Eq. (14) associated with the changing electron density in the sheath produce larger sheaths than predicted by earlier models. In some cases, the extra terms of Eq. (14) become so important that the rate of sheath growth can become too large to

be resolved accurately by PIC/CLO. In regimes of rapid sheath growth, ions cannot equilibrate, and the use of the bipolar estimate for the ion current density [Eq. (36)] becomes increasingly inaccurate.

In comparing results from PIC/CLO and the modified bipolar model with results from earlier models, a refined version of the model provided by Eqs. (1) - (3) is used to represent earlier sheath opening treatments. This refinement modifies Eqs. (1) - (3) to include the non-zero ion injection velocities and relativistic voltages allowed here. The extension of earlier treatments is identical to the modified bipolar model of Sec. V, except that the original sheath opening equation, Eq. (3) is used rather than Eq. (35). Explicitly stated, the model used to represent earlier treatments employs the combination of Eqs. (38), (36), and (3), with $j_i^{BP}(t)$ given by Eq. (29), and with the usual boundary conditions on $\gamma(x,t)$. Like PIC/CLO and the modified bipolar model, this model is driven by $j_b(t)$ and output includes the time dependent sheath size and potential.

Unless otherwise specified, in each of the figures below curve (a) represents the PIC/CLO result, curve (b) the modified bipolar model, and curve (c) the earlier treatments. When a curve is labelled with a number rather than a letter, it represents the output from one of the five cases listed in Table I. Thus a curve labelled 4b means that the modified bipolar model has been applied to case 4 in order to produce the result displayed.

First the electrical chararcteristics of each case will be described. Summaries of these characteristics from PIC/CLO, together with the sheath sizes at t_o are given in Table I. The growth of the sheath potential in time is shown in Figs. 2 - 6 for each of the five cases. Also shown is the driving beam current density in each case. The three potential plots in each figure represent the three models discussed in this work. As can be seen in the figures, very good agreement is generally found between the modified

bipolar model and PIC/CLO. In cases 1 - 3, discrepancies of 20-30% exist between PIC/CLO and the earlier treatments. In regimes of lower density, higher rate of current density rise such as cases 4 and 5, differences of factors between 4 and 10 become apparent, as seen in Figs. 5 and 6. The differences between PIC/CLO and earlier models are also demonstrated in Fig. 7, where the time dependent ratio, $\phi(x_s,t)/j_b(t)$ is plotted for cases 2 and 5 in units of Ω–cm^2.

Sheath growth for each of the five cases is shown in Figs. 8 - 12. The same comments made above for the potential growth apply here, where differences of approximately 25% exist between PIC/CLO and the earlier models in the higher density regimes, but large discrepancies (factors of 4 - 10) are seen in lower density, higher current density rise regimes (i.e. cases 4 and 5). The modified bipolar model again improves substantially on the earlier models. Curve (a) in Fig. 12 shows oscillations that are the result of numerical noise and that should not be taken literally.

A summary of how the models differ in their treatment of sheath growth illustrates why this rapid sheath growth occurs in the new models presented here. Starting with earlier treatments, the sheath size was determined by dropping the last two terms of Eq. (14) and assuming that $j_i(0,t) = j_i^{BP}(t)$, so that,

$$\dot{x}_s = \frac{\left|j_i^{BP}(t)\right|}{Zen_o} - u_o \,. \tag{41}$$

The modified bipolar model improves on this by dropping only the last term of Eq. (14), giving Eq. (35), with $j_i(0,t) = j_i^{BP}(t)$. Finally, PIC/CLO retains all the terms of Eq. (14) and calculates $j_i(0,t)$ independently of $j_i^{BP}(t)$, giving,

$$\dot{x}_s = \frac{\left|j_i(0,t)\right| - Zen_o u_o + \Delta j_b}{Zen_o + \rho_b(x_s,t)}\,, \tag{42}$$

with Δj_b given by Eq. (13). As demonstrated in Figs. 8 - 12, PIC/CLO and the modified bipolar models always show larger sheath growth than earlier models, sometimes by an order of magnitude. The reason for this is largely because of the $\rho_b(x_s,t)$ term in the denominator of Eq. (42). Because ρ_b is negative, the effect of this term on sheath growth is to reduce the denominator of Eqs. (42) and (35) compared with that of Eq. (41), and thus increase $\dot{x}_s$. Another reason for larger sheath growth is the term Δj_b, which is always positive for the cases here with rising $|j_b|$.

The next four figures depict the spatial profiles of the potential and number densities comparing cases 2 and 5 for the PIC/CLO and modified bipolar models. In these figures, n_b is the beam density and Zn_i is the ion charge state times the ion density. Figure 13 shows the PIC/CLO results for case 2 at t = 10 ns. . This should be compared with the modified bipolar results for the same case and time in Fig. 14. The largest difference is between the estimates of the ion density at the sheath/plasma boundary. Because the region of disagreement in the ion density is small, the potentials calculated by the two models agree very well. Sheath growth in case 2 is relatively slow, giving good agreement between the models. With rapid sheath growth in case 5, larger differences are found. In Fig. 15, the potential and density profiles from PIC/CLO are shown for case 5 at t = 2 ns. These can be compared with the modified bipolar model in Fig. 16, where the ion density plot is truncated for clarity. At the last data point, $x = x_s$, $Zn_i = 7.1 \times 10^{13}$ cm^{-3} . Despite large discrepancies in the sheath size and ion density near the sheath/plasma boundary, the modified bipolar model provides a fairly good estimate (within 25%) of the sheath potential.

Figure 15 demonstrates that large sheath growth is seen in cases when $\rho_b(x_s,t) \rightarrow -Zen_o$. Further illustration of this point, and a comparison among cases is given in Fig. 17, where the time dependence of the beam density, $n_b(x_s,t)$ is plotted for the three 10^{12} cm^{-3} cases, 2, 4 and 5. The curves are labelled by their case numbers and

by their rates of beam current density rise. If the traces were to reach $Zn_o = 2 \times 10^{12}$ cm^{-3}, the sheath growth rate predicted by either Eqs. (42) or (35) would be infinite. Table I gives the value of $n_b(x_s)$ at the stopping time for all five cases. This number should be compared with Zn_o for the case in question.

An explanation of why $\rho_b(x_s,t) \rightarrow -Zen_o$ in some cases can understood from the following argument. If it is assumed that the ion charge density is roughly uniform, Eq. (34) can be integrated once to yield an expression related to the electric field through Eq. (19). The boundary condition that the electric field vanish at the sheath edge then gives

$$j_b = -n_o eZc\sqrt{\frac{\gamma_o - 1}{\gamma_o + 1}}. \tag{43}$$

This result relates the beam current density to the sheath voltage in the ion matrix limit. Using Eq. (20) to relate j_b and ρ_b, an expression is obtained for the electron density at the sheath edge,

$$\rho_b(x_s) = -n_o eZ\frac{\gamma_o}{\gamma_o + 1}. \tag{44}$$

In the non-relativistic limit, the beam charge density approaches $n_o eZ/2$, giving a factor of two increase in sheath growth over that predicted by Eq. (41). Equation (44) shows that in the limit of large sheath potential (i.e. $\gamma_o >> 1$), $\rho_b(x_s,t) \rightarrow -Zen_o$, and Eq. (42) would predict explosive sheath growth. This result shows that explosive sheath growth is a relativistic effect on the beam electron density. Although the resulting sheath growth singularity is quite interesting, it cannot be taken too literally. First of all, the large beam density in this limit almost removes the distinction between the sheath and plasma. Secondly, there is the question of electron inertia effects. In the two examples above that exhibited this singularity, the simulations were stopped before such effects became important. If they had been allowed to continue, the sheath velocity would become so

extreme that electron energy conservation would no longer be conserved, and the electron current density would be strongly non-uniform. In this limit, Eq. (20) would no longer be a good estimate of the electron charge density and the models considered here would break down. On this issue, Table I can be used to estimate this error. Dividing Δj_b by $|j_b(t_o)|$ gives the degree of non-uniformity in the electron current density for each case. For case 1, this ratio is 6×10^{-4}, while for case 5 it is 6.3×10^{-2} at $t = t_o$.

In the next three pairs of figures, further comparisons of cases 2 and 5 are made to demonstrate the effects of ion inertia. In Figs. 18 and 19, spatial profiles of the ion current density are shown for these two cases. In each case, the modified bipolar model overestimates $|j_i(x)|$, especially near x_s, leading to the error in ρ_i mentioned in the discussion of Figs. 14 and 16. This error is also implicitly made in earlier models of sheath growth where the ion current density is also assume uniform. Ion inertia effects can be seen by comparing the profiles of the curves labelled (a) in these two figures. In Fig. 18, where inertia effects are small, the ion current density predicted by PIC/CLO rises to about 90% of the modified bipolar value at the cathode. In case 5, where the sheath grows so rapidly that ions cannot respond and equilibrate, the current density profile predicted by PIC/CLO rises to only about 60% of the modified bipolar value at the cathode. Thus, it is seen that ion inertia manifests itself by reducing the magnitude of $|j_i(0,t)| - Zen_o u_o$ compared with $|j_i^{BP}(t)| - Zen_o u_o$. According to Eqs. (42) or (35), these results would suggest smaller sheath growth would be predicted by PIC/CLO than the modified bipolar model. As will be shown shortly, the opposite result holds because the addition of Δj_b to Eq. (42) more than offsets any ion inertia effects. In Table I, ion current density results are summarized for all five cases. Both $j_i(0,t_o)$ from PIC/CLO, and $j_i^{BP}(t_o)$ from the modified bipolar model (MBP) are tabulated. Note that $j_i^{BP}(t_o)$ from the modified bipolar model is based on the voltages predicted in that model. For comparison, $j_i^{BP}(t_o)$ using the voltages from PIC/CLO (PIC) are also shown in Table I.

These value of $|j_i^{BP}(t_o)|$ are larger than those from the modified bipolar model, especially in cases 4 and 5. The differences between $j_i^{BP}(t_o)$(PIC) and $j_i(0,t_o)$ show how far from equilibrium these solutions really are.

Time histories of $j_i(0,t)$ are shown from cases 2 and 5 in Figs. 20 and 21. As usual, curves (a) and (b) refer to the results from PIC/CLO and the modified bipolar model respectively. However, curve (c) in this case is not the result from earlier models, but the last term of Eq. (42), $\Delta j_b \equiv -\int_0^{x_s} \frac{\partial \rho_b}{\partial t} dx$. This term has been included in this figure because its importance to Eq. (42) can be judged by comparing its magnitude with $j_i(0,t)$. Figure 20 shows that, in case 2, Δj_b is a small fraction of the ion current density, and that good agreement exists between the PIC/CLO cathode ion current density and the modified bipolar estimate. Figure 21, from case 5 shows larger differences (factors of 1.7) between the two estimates of $j_i(0,t)$, and an overwhelming contribution to Eq. (14) from Δj_b. These results support the point made earlier that ion inertia effects are offset by the contribution of Δj_b to Eq. (42), producing larger sheath growth in PIC/CLO than in the modified bipolar model. $\Delta j_b(t_o)$ is shown in Table I for each of the five cases. Its importance to Eq. (42) can be judged by comparing its magnitude with $|j_i(0,t_o)| - Zen_o u_o$. The large values of Δj_b in cases 4 and 5 in concert with small values of $Zen_o - en_b(x_s,t)$ produce the large sheath growth in those cases.

In an attempt to understand how ion inertial effects influence estimates of $j_i(0,t)$, the terms of Eq. (28) from cases 2 and 5, as calculated by PIC/CLO, are plotted in Figs. 22 and 23. Curves (a) - (d) are the second, third, and fourth terms on the right of Eq. (28) and their sum, all normalized to $j_i^{BP}(t)$. Thus, Eq. (28) would be written $j_i(0,t) \cong j_i^{BP}(t)[1-(a)-(b)-(c)] = j_i^{BP}(t)[1-(d)]$. Figure 22 shows that in case 2, good agreement between $j_i(0,t)$ and $j_i^{BP}(t)$ is obtained because of cancellation among the terms. Such cancellation does not occur in case 5, as seen in Fig. 23 where curve (a)

dominates the others. Figure 23 shows that ion inertial effects are much more important in case 5 than in case 2. Additional support for this conclusion is given by a diagnostic built into PIC/CLO that compares the actual $v_i(0,t)$ at the cathode with the velocity predicted by the ion conservation of energy equation given in Eq. (27). This diagnostic shows that Eq. (27) overestimates the actual ion velocity at the cathode by 40% in case 2, and by a factor of 6 in case 5 at the respective stopping times in each case.

VIII. Conclusions

In this paper, the dynamic behavior of bipolar plasma sheaths has been examined. The models presented here assume that electrons evolve in a series of quasi-equilibrium states so that, to good approximation, electron energy is conserved and the electron current density is uniform in the calculation of the electric field and electron charge density. The analysis is one dimensional and magnetic field effects are neglected. Earlier models of sheath growth share these assumptions with the present treatment. The former models, however, assume that ions also evolve in a series of quasi-equilibria so that the equilibrium bipolar Child-Langmuir equations hold. Equations (1) - (3) express the resulting sheath opening dynamics. The treatment introduced here builds on earlier methods in a three ways. First of all, analytic generalizations of Eqs. (2) and (3) are developed, resulting in Eqs. (24) and (14). Secondly, the modified bipolar model is developed, which retains the ion equilibrium assumptions in the calculation of the sheath potential, but adds terms to Eq. (3) to make the sheath growth equation more consistent with the full ion continuity equation, Eq. (14). In this way, uniform ion current density is assumed in the potential calculation, but not in the ion continuity equation. Thirdly, the PIC/CLO model described here drops the ion equilibrium assumptions and resolves ion inertial effects. Sheath opening is fully consistent with the ion continuity equation, and hence Eq. (14).

It has been found that earlier models neglect effects that manifest themselves even in regimes where ions dynamics can be treated as a series of quasi-equilibrium states. This error results in underestimates of the actual sheath size and potential. In the higher density regimes of 10^{13} cm^{-3}, actual sheath sizes and potentials are about 25% higher than earlier estimates, while at the lower density of 10^{12} cm^{-3}, sheaths sizes and potentials can be factors of 1.5 to 10 times larger than earlier models predict, depending on the rate of rise of the driving current density. The discrepancies with earlier models occur largely because of the neglect of terms in the sheath opening equation related both to electron charge density and to electron dynamics. Electron charge density at the sheath edge reduces the denominator in Eq. (42) compared with Eq. (41), thus increasing $\dot{x}_s$. Electrons respond to the rising demand for current density by redistributing themselves in the sheath in such a way that, in certain regimes, $\rho_b(x_s,t) \rightarrow -Zen_o$ and Δj_b becomes important. Thus, the inclusion of electron dynamic effects allows for the possibility of singular sheath growth. However, extreme growth taxes the credibility of the models employed here because electron inertia effects also become important when sheaths grow too fast. In the results presented here, calculations have been stopped before the electron energy conservation and continuity equations are strongly violated, but the trend toward very rapid sheath growth is apparent.

Ion inertia effects manifest themselves by reducing the magnitude of the ion current density in the sheath compared with the bipolar value, $|j_i^{BP}|$, to which the ions tend in the limit of slow sheath growth (i.e. $\tau_i << \tau_s$). These effects were demonstrated in Figs. 18 and 19. Figure 18 is typical of the cases 1 - 3, where ion inertia effects are small and $|j_i(0,t)|$ almost reaches $|j_i^{BP}|$. Figure 19 is representative of cases 4 and 5, where sheath growth becomes so large that $|j_i(0,t)|$ reaches only about halfway between Zen_ou_o and $|j_i^{BP}|$. This trend can be taken to the ion matrix limit, where $|j_i(0,t)| \rightarrow Zen_ou_o$. According to Eq. (42), therefore, ion inertia effects manifest themselves by reducing the

ion current density contribution to sheath growth [the first two terms in the numerator of Eq. (42)].

Several important effects have been left untreated in this paper. The effect of magnetic fields and inductive electric fields should be included in future work. The interaction of the emitted electron beam with the background plasma (producing instabilities) or with a neutral gas (producing ionization effects) would also significantly modify the results presented here.

IX. Acknowledgements

The authors gratefully acknowledge many stimulating discussions with Dr. James Geary and Dr. Robert Kares of Berkeley Research Associates, Dr. John Goyer of Physics International Company, and with members of the Pulsed Power Physics branch at the Naval Research Laboratory.

This work was supported by the U. S. Office of Naval Research.

X. References

[1]D. Bohm, in *Characteristics of Electrical Discharges in Magnetic Fields*, edited by A. Guthrie and R.K. Wakering (McGraw Hill, New York, 1949), Chapter 3.
[2]I. Langmuir, Phys. Rev., 33, 954 (1929).
[3]J.W. Cipolla and M.B. Silevitch, J. Plasma Physics, 25 (3), 373 (1981).
[4]K.F. Sander, J. Plasma Physics, 3 (3), 353 (1969).
[5]J.G. Andrews and R.H. Varey, Phys. of Fluids, 14 (2), 339 (1970).
[6]V.L. Bailey, J.M. Creedon, B.M. Ecker, and H.I. Helava, J. Appl. Phys., 54 (4), 1656 (1983).
[7]P.C. Stangeby, Phys. of Fliuds, 27 (3), 682 (1983).
[8]A. Mentze, D.W. Ernie, and H.J. Oskam, J. Appl. Phys., 60 (9), 3081 (1986).
[9]A.C. Calder and J.G. Laframboise, Phys. of Fluids B, 2 (3), 655 (1990).
[10]P.A. Miller, J.W. Poukey, and T.P. Wright, Phys. Rev. Letters, 35 (14), 940 (1975).
[11]P.F. Ottinger, S.A. Goldstein, and R.A. Meger, J. Appl. Phys., 56 (3), 774 (1984).
[12]V.W. Koch, Z. Tech. Phys, 17, 446 (1936).
[13]C.D. Child, Phys. Rev., 32, 492 (1928).
[14]M. Widner, I. Alexeff, W.D. Jones, and Lonngren, Phys. of Fluids, 13 (10), 2532 (1976).
[15]C.W. Mendel and S.A. Goldstein, J. Appl. Physics, 48 (3), 1004 (1977).
[16]J.M. Creedon, J. Appl. Phys., 46, 2946 (1975).

[17]R.J. Kares, Berkeley Research Technical Report No. BRA-90-360R, (1990). R.J. Kares, J. Geary, J.M. Grossmann, Berkeley Research Technical Report No. BRA-91-361R, (1991).
[18]A. Kadish, P. William, and M.E. Jones, Appl. Phys. Letters, **47**, 115 (1985).
[19]C.K. Birdsall and A.B. Langdon, "Plasma Physics via Computer Simulation", McGraw-Hill, 1985.
[20]J.M. Grossmann, J.M. Neri, P.F. Ottinger, and A.T. Drobot, Phys. Fluids **29**, 2724, (1986).

case	1	2	3	4	5
$n_o(\times 10^{12}\mathrm{cm}^{-3})$	10	1	10	1	1
u_o (cm/μ s)	1	10	1	10	10
$\mid dj_b/dt \mid$ (KA/cm^2-ns)	0.1	0.1	1.0	1.0	4.0
t_o (ns)	10	10	10	6.5	2
$\mid j_b(t_o) \mid$ (KA/cm^2)	1.34	1.34	10.34	6.8	8.34
$x_s(t_o)$ (cm)	0.024	0.37	0.21	3.2	4.0
$\phi(x_s, t_o)$ (KV)	2.75	92	197	4450	4330
$\mid j_i(0, t_o) \mid$ (A/cm^2)	12.8	13.2	102	82	56
$\mid j_i^{BP}(t_o) \mid$ (A/cm^2)(MBP)	13.4	14.1	106	95.7	94.3
$\mid j_i^{BP}(t_o) \mid$ (A/cm^2)(PIC)	13.4	14.2	108	174	161
$\Delta j_b(t_o)$ (A/cm^2)	0.8	2.4	11.7	123	526
$n_b(x_s, t_o)$ ($\times 10^{12}\mathrm{cm}^{-3}$)	2.7	0.53	3.1	1.43	1.75

TABLE I. Parameters used in the five cases treated in this paper. Rows 1 - 5 are input parameters , rows 6- 12 are output results. All of the results are from PIC/CLO, except the row labelled $\left|j_i^{BP}(t_o)\right|$(MBP), which is the ion current density from the modified bipolar model.

TABLE CAPTION

TABLE I. Parameters used in the five cases treated in this paper. Rows 1 - 5 are input parameters , rows 6- 12 are output results. All of the results are from PIC/CLO, except the row labelled $\left|j_i^{BP}(t_o)\right|$(MBP), which is the ion current density from the modified bipolar model.

FIGURE CAPTIONS

FIG. 1. Schematic of a one dimensional dynamic bipolar sheath. n_o is the plasma ion density and u_o is the plasma injection speed.

FIG. 2. Current density and sheath potential histories for case 1, a 10^{13} cm^{-3} plasma driven with a beam current density rise of -0.1 KA/cm^2-ns. Labels (a), (b), and (c) refer to the PIC/CLO, modified bipolar, and earlier models, respectively.

FIG. 3. Current density and sheath potential histories for case 2, a 10^{12} cm^{-3} plasma driven at a rate of -0.1 KA/cm^2-ns.

FIG. 4. Current density and sheath potential histories for case 3, a 10^{13} cm^{-3} plasma driven at a rate of -1.0 KA/cm^2-ns.

FIG. 5. Current density and sheath potential histories for case 4, a 10^{12} cm^{-3} plasma driven at a rate of -1.0 KA/cm^2-ns.

FIG. 6. Current density and sheath potential histories for case 5, a 10^{12} cm^{-3} plasma driven at a rate of -4.0 KA/cm^2-ns.

FIG. 7. Ratio of sheath potential to beam current density for cases 2 and 5, where a 10^{12} cm^{-3} plasma is driven at a rates of -0.1 KA/cm^2-ns and -4.0 KA/cm^2-ns, respectively. Curves labelled (a) and (c) refer to the PIC/CLO and earlier models, respectively.

FIG. 8. Sheath size evolution for case 1, a 10^{13} cm^{-3} plasma driven at a rate of -0.1 KA/cm^2-ns. As before, labels (a), (b), and (c) refer to the PIC/CLO, modified bipolar, and earlier models, respectively.

FIG. 9. Sheath size evolution for case 2, a 10^{12} cm^{-3} plasma driven at a rate of -0.1 KA/cm^2-ns.

FIG. 10. Sheath size evolution for case 3, a 10^{13} cm^{-3} plasma driven at a rate of -1.0 KA/cm^2-ns.

FIG. 11. Sheath size evolution for case 4, a 10^{12} cm^{-3} plasma driven at a rate of -1.0 KA/cm^2-ns.

FIG. 12. Sheath size evolution for case 5, a 10^{12} cm^{-3} plasma driven at a rate of -4.0 KA/cm^2-ns.

FIG. 13. Profiles of the potential, and electron and ion densities in the sheath at time t_o = 10 ns from the PIC/CLO model for case 2, a 10^{12} cm^{-3} plasma driven at a rate of -0.1 KA/cm^2-ns.

FIG. 14. Profiles of the potential, and electron and ion densities in the sheath at time t_o = 10 ns from the modified bipolar model for case 2, a 10^{12} cm^{-3} plasma driven at a rate of -0.1 KA/cm^2-ns.

FIG. 15. Profiles of the potential, and electron and ion densities in the sheath at time t_o = 2 ns from the PIC/CLO model for case 5, a 10^{12} cm^{-3} plasma driven at a rate of -4.0 KA/cm^2-ns.

FIG. 16. Profiles of the potential, and electron and ion densities in the sheath at time t_o = 2 ns from the modified bipolar model for case 5, a 10^{12} cm^{-3} plasma driven at a rate of -4.0 KA/cm^2-ns.

FIG. 17. History of the beam density at the sheath/plasma boundary for cases 2, 4 , and 5, where a 10^{12} cm^{-3} plasma is driven with the rates of beam current density rise shown.

FIG. 18. Profile of the ion current density in the sheath at t_o = 10 ns for case 2, a 10^{12} cm^{-3} plasma driven at a rate of -0.1 KA/cm^2-ns. Curves labelled (a) and (b) refer to the PIC/CLO and the modified bipolar models respectively. The curves end at the sheath/plasma boundary predicted by each model.

FIG. 19. Profile of the ion current density in the sheath at t_o = 2 ns for case 5, a 10^{12} cm^{-3} plasma driven at a rate of -4.0 KA/cm^2-ns. Curves labelled (a) and (b) refer to the PIC/CLO and the modified bipolar models respectively. The curves end at the sheath/plasma boundary predicted by each model.

FIG. 20. Histories of the ion current density at the cathode and term Δj_b of Eq. (13) for case 2, a 10^{12} cm^{-3} plasma driven at a rate of -0.1 KA/cm^2-ns. Curves (a) and (b) refer to the PIC/CLO and modified bipolar model predictions of $j_i(0,t)$, while curve (c) is the term Δj_b from PIC/CLO.

FIG. 21. Histories of the ion current density at the cathode and term Δj_b of Eq. (13) for case 5, a 10^{12} cm^{-3} plasma driven at a rate of -4.0 KA/cm^2-ns. Curves (a) and (b) refer to the PIC/CLO and modified bipolar model predictions of $j_i(0,t)$, while curve (c) is the term Δj_b from PIC/CLO.

FIG. 22. Histories of the three terms on the right of j_i^{BP} in Eq. (28) [curves (a) - (c)], and their sum [curve (d)], all normalized to j_i^{BP}. Curves are from case 2, a 10^{12} cm^{-3} plasma driven at a rate of -0.1 KA/cm^2-ns, using PIC/CLO.

FIG. 23. Histories of the three terms on the right of j_i^{BP} in Eq. (28) [curves (a) - (c)], and their sum [curve (d)], all normalized to j_i^{BP}. Curves are from case 5, a 10^{12} cm^{-3} plasma driven at a rate of -4.0 KA/cm^2-ns, using PIC/CLO.

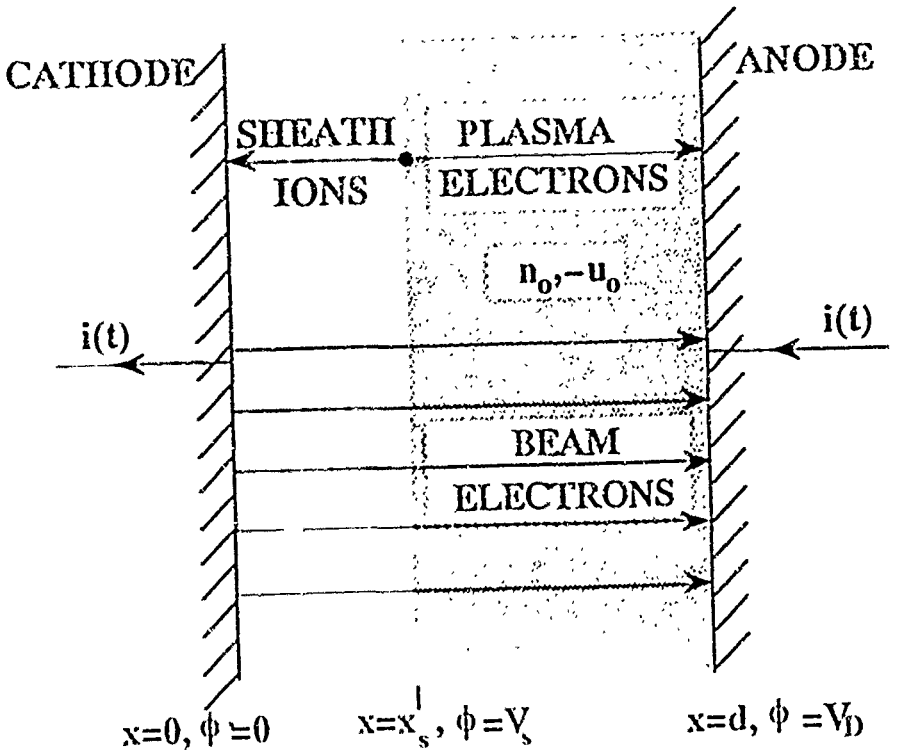
CATHODE
ANODE
SHEATH
PLASMA
IONS
ELECTRONS
$n_0, -u_0$
i(t)
i(t)
BEAM
ELECTRONS
x=0, ϕ =0
x=x_s', ϕ =V_s
x=d, ϕ =V_D

FIG. 1

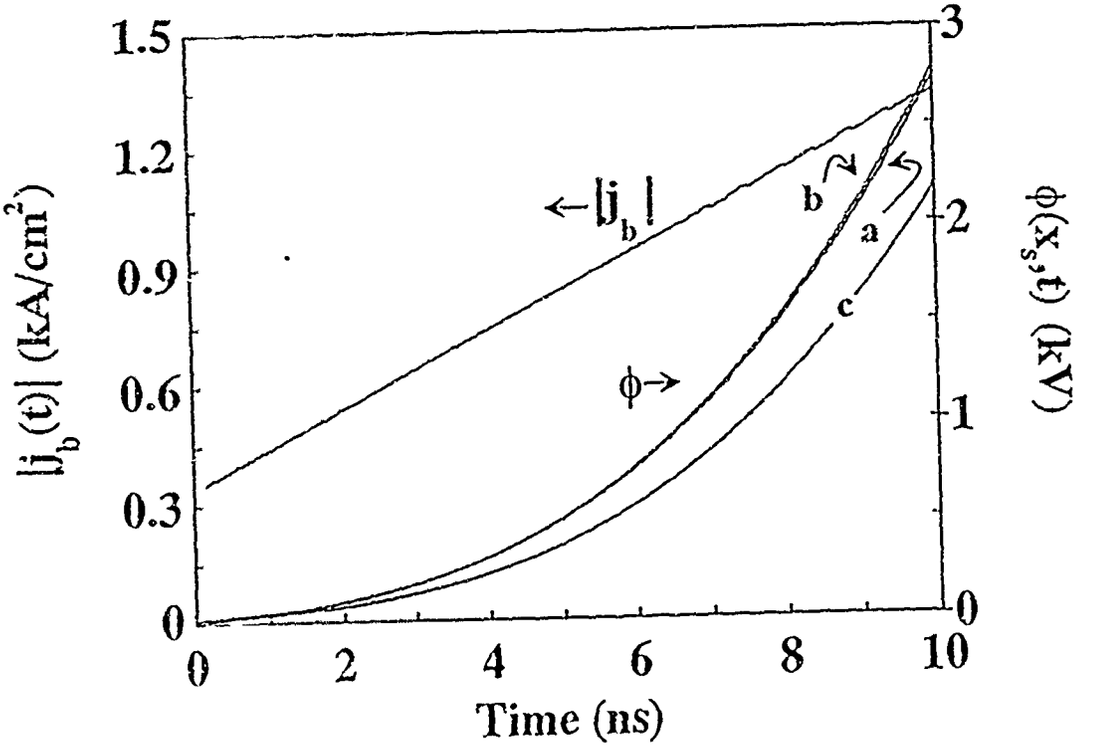
1.5
1.2
0.9
0.6
0.3
0
3
2
1
0
0
2
4
6
8
10
Time (ns)
$|j_b(t)|$ (kA/cm^2)
$\phi(x_s,t)$ (kV)
$\leftarrow |j_b|$
$\phi \rightarrow$
a
b
c

FIG. 2

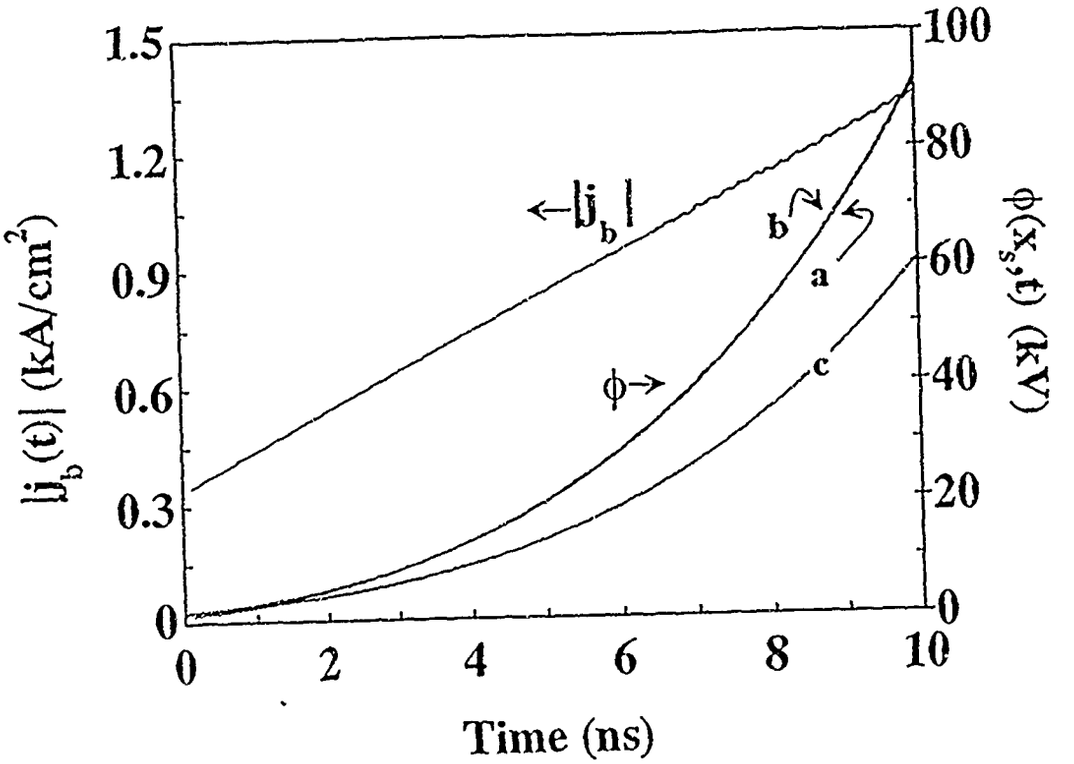
1.5
1.2
0.9
0.6
0.3
0
0
2
4
6
8
10
100
80
60
40
20
0
$|j_b(t)|$ (kA/cm^2)
$\phi(x_s,t)$ (kV)
Time (ns)
$\leftarrow|j_b|$
$\phi\rightarrow$
a
b
c

FIG. 3

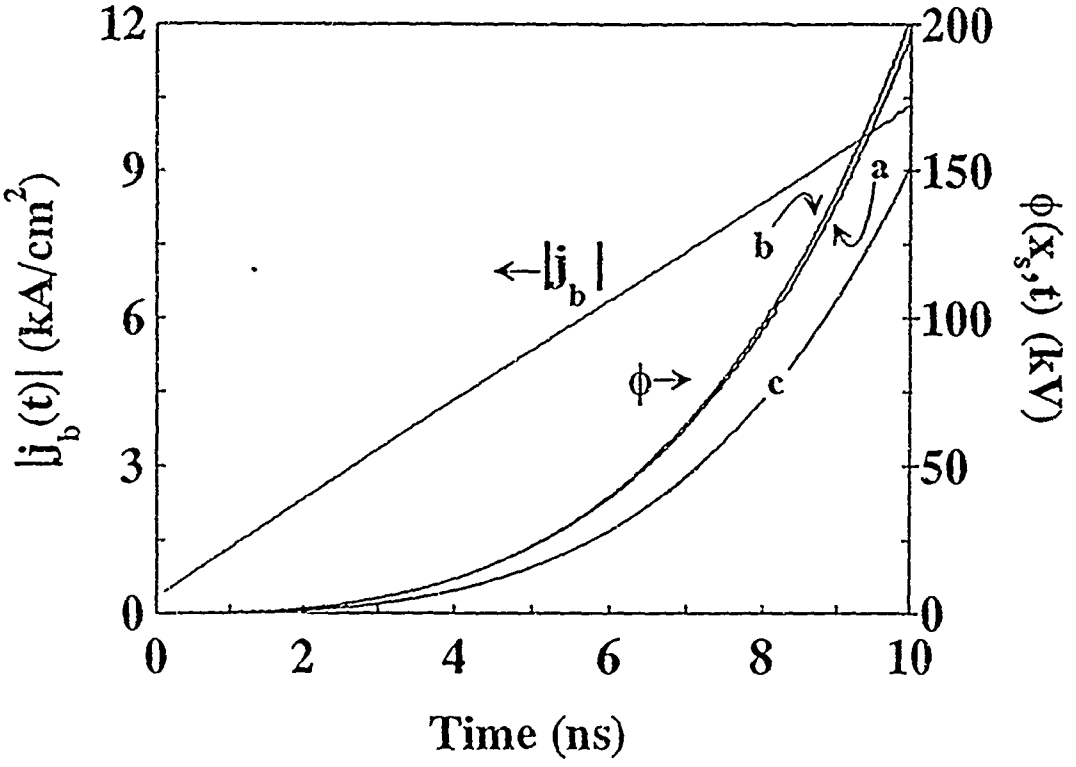
12
9
6
3
0
200
150
100
50
0
0
2
4
6
8
10
Time (ns)
$|j_b(t)|$ (kA/cm^2)
$\phi(x_s,t)$ (kV)
$\leftarrow|j_b|$
$\phi\rightarrow$
a
b
c

FIG. 4

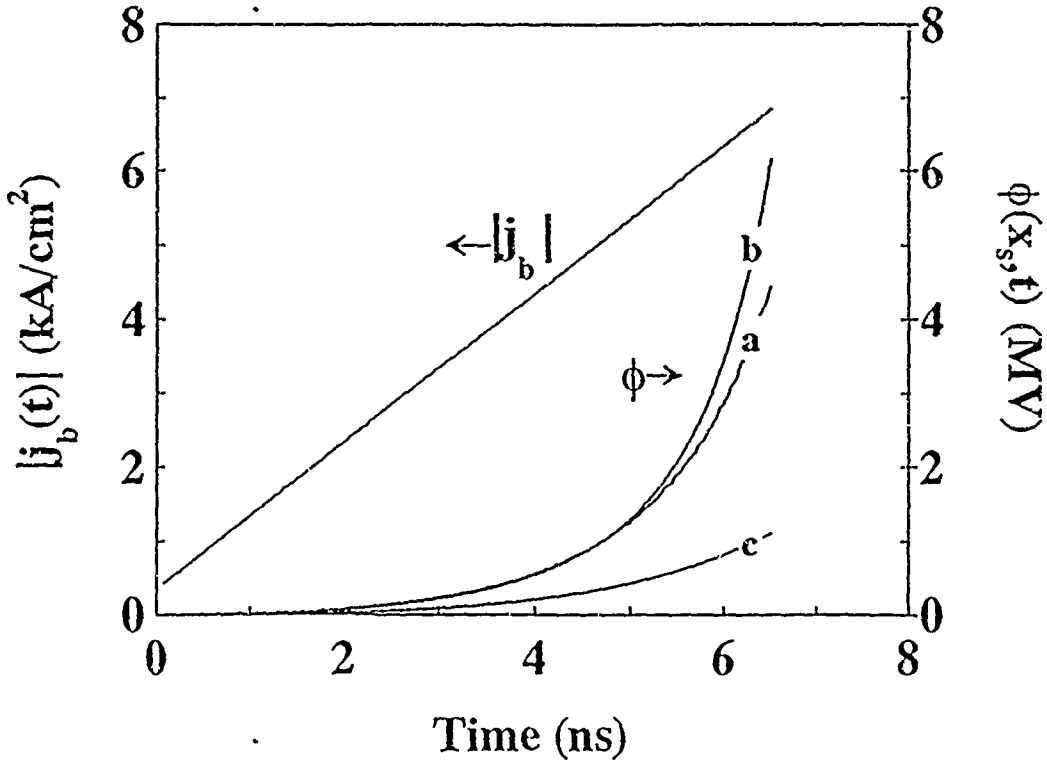
8
6
4
2
0
0
2
4
6
8
$|j_b(t)|$ (kA/cm^2)
$\phi(x_s,t)$ (MV)
Time (ns)
$\leftarrow|j_b|$
$\phi\rightarrow$
b
a
e

FIG. 5

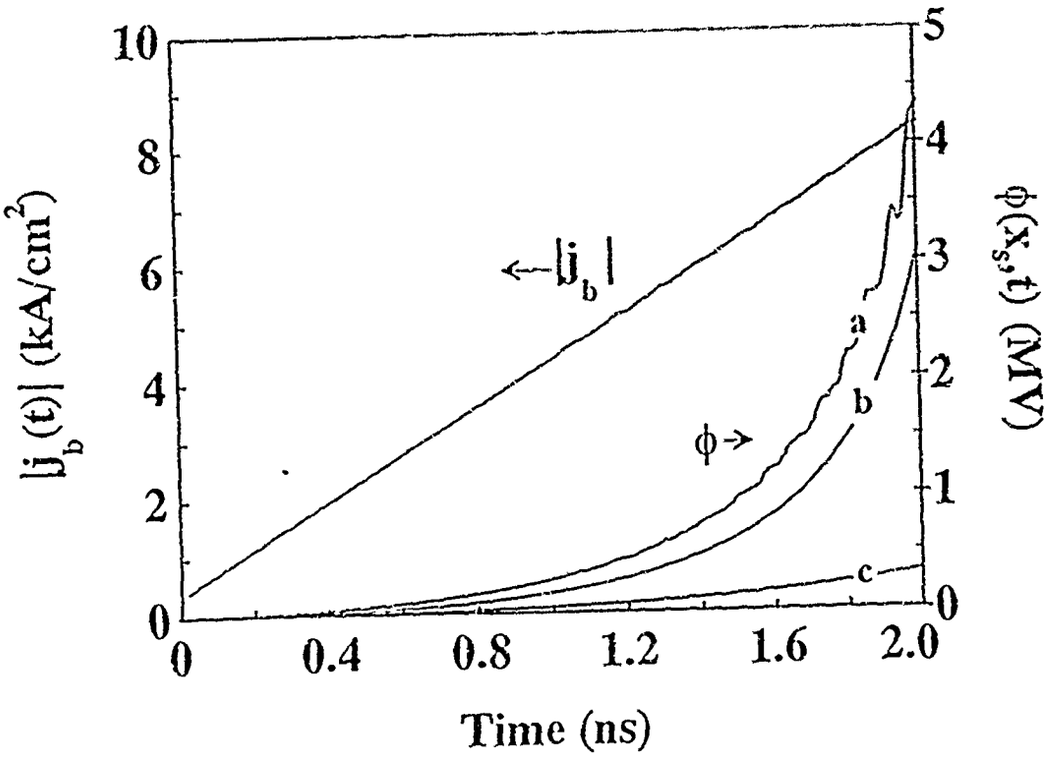
10
8
6
4
2
0
0
0.4
0.8
1.2
1.6
2.0
Time (ns)
$|j_b(t)|$ (kA/cm^2)
$\phi(x_s,t)$ (MV)
5
4
3
2
1
0
$\leftarrow |j_b|$
$\phi \rightarrow$
a
b
c

FIG. 6

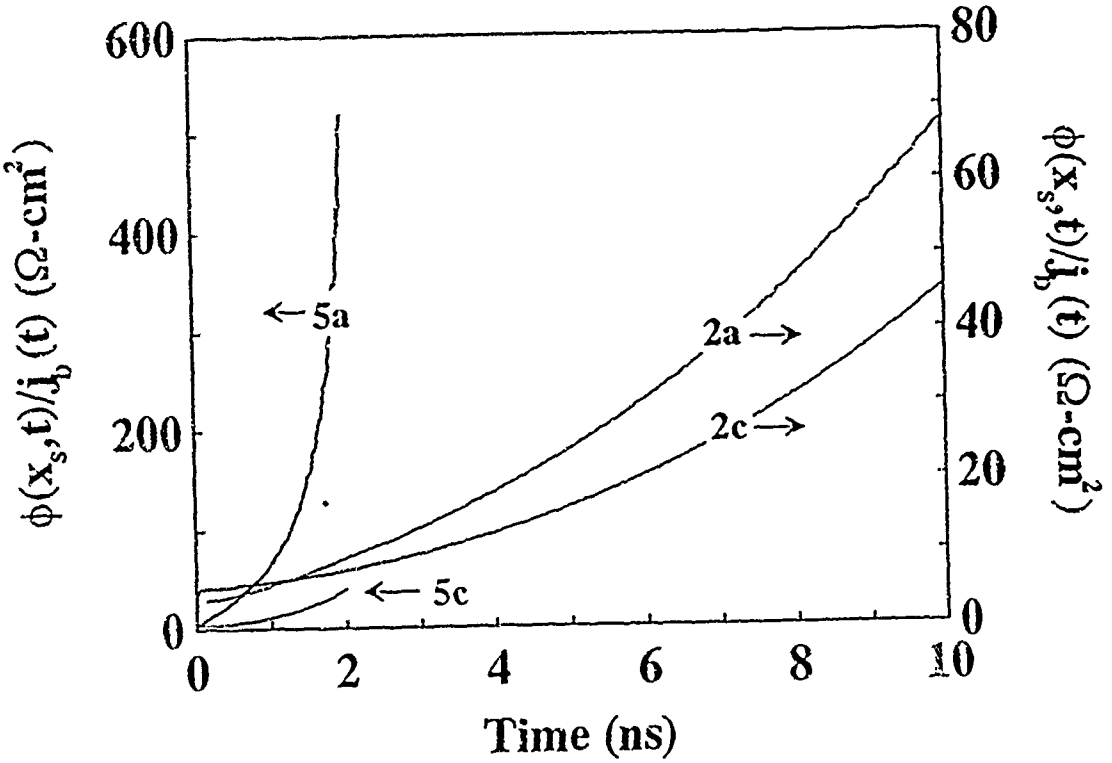
600
400
200
0
80
60
40
20
0
0
2
4
6
8
10
Time (ns)
$\phi(x_s,t)/j_b(t)$ (Ω-cm^2)
$\phi(x_s,t)/j_b(t)$ (Ω-cm^2)
5a
2a
2c
5c

FIG. 7

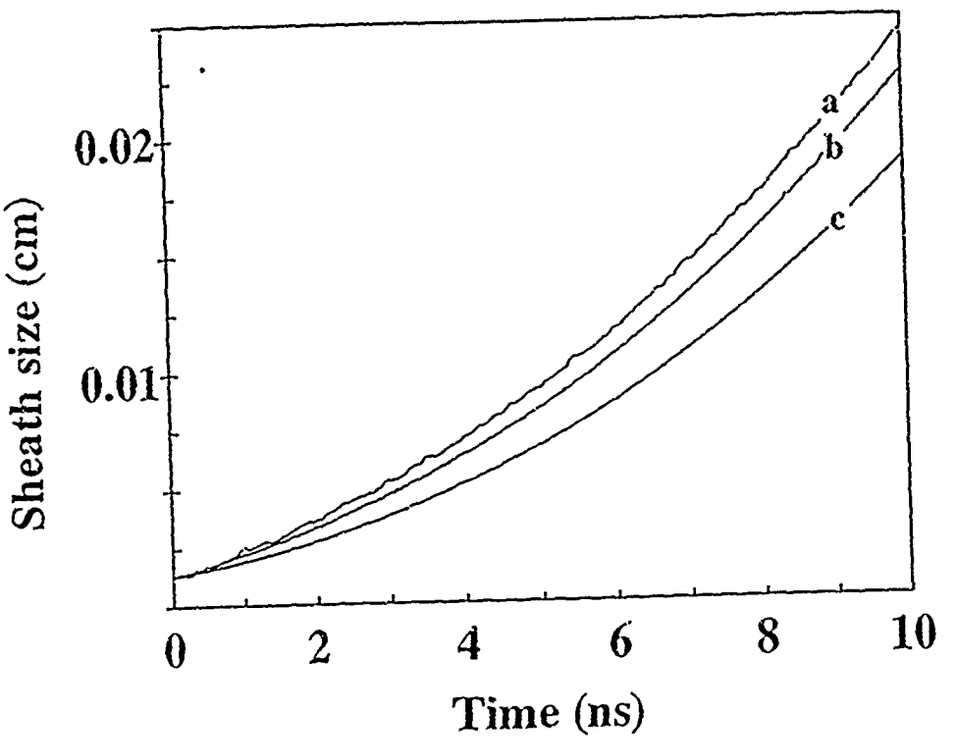

FIG. 8

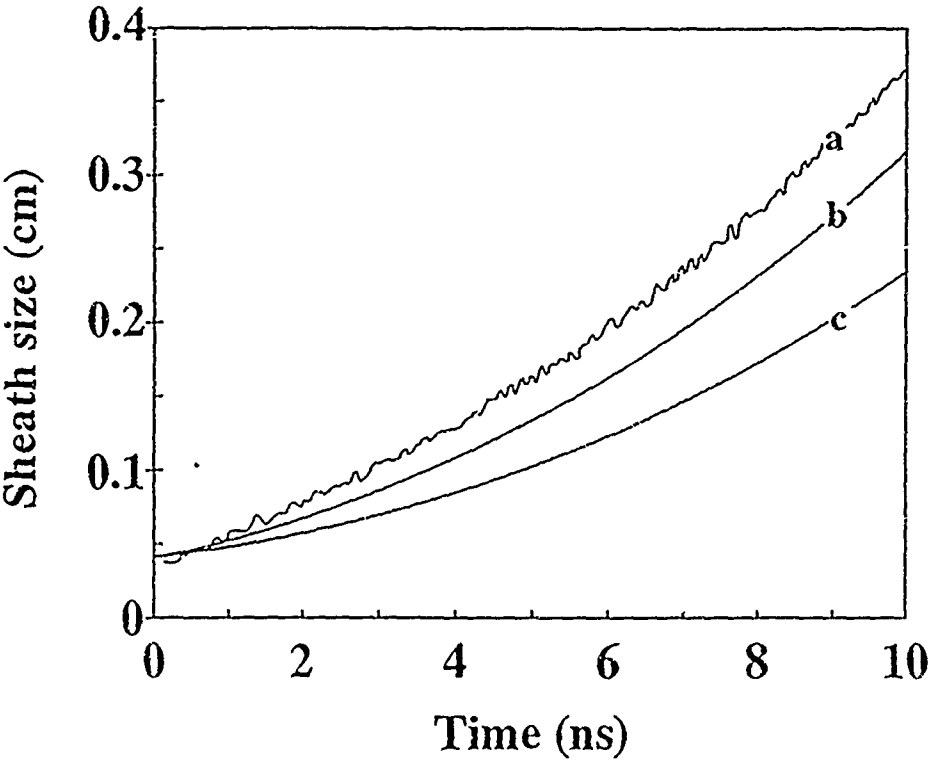

FIG. 9

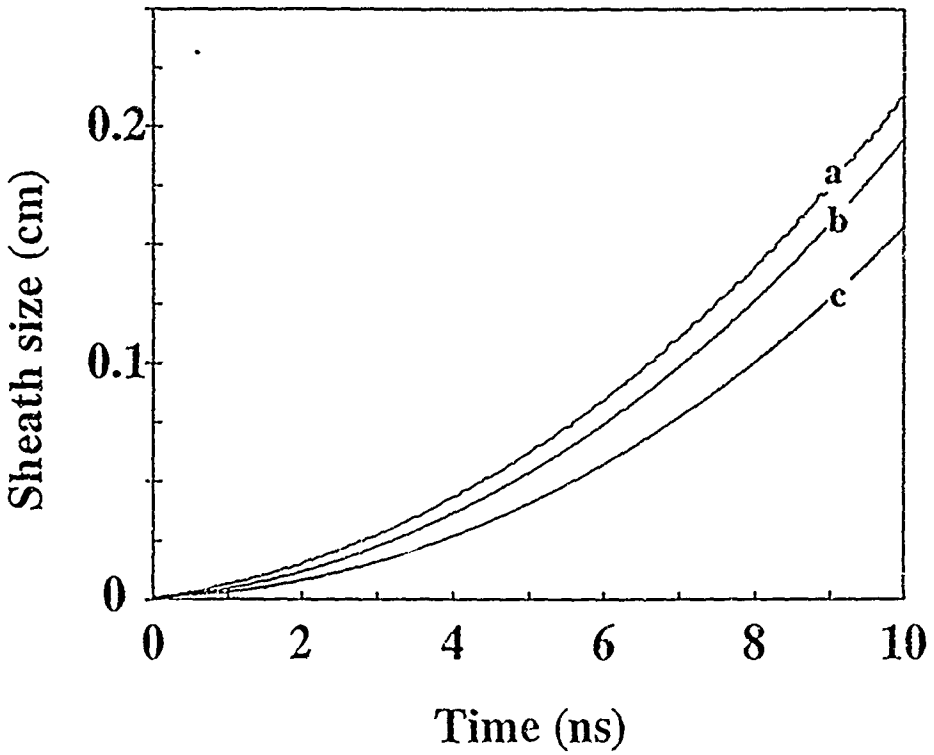

FIG. 10

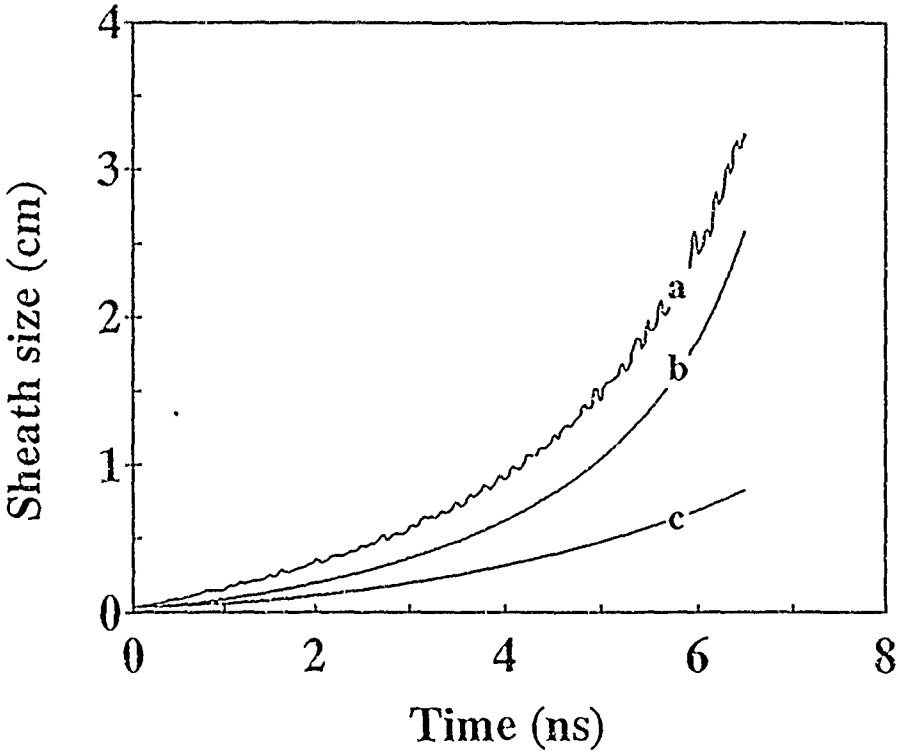

FIG. 11

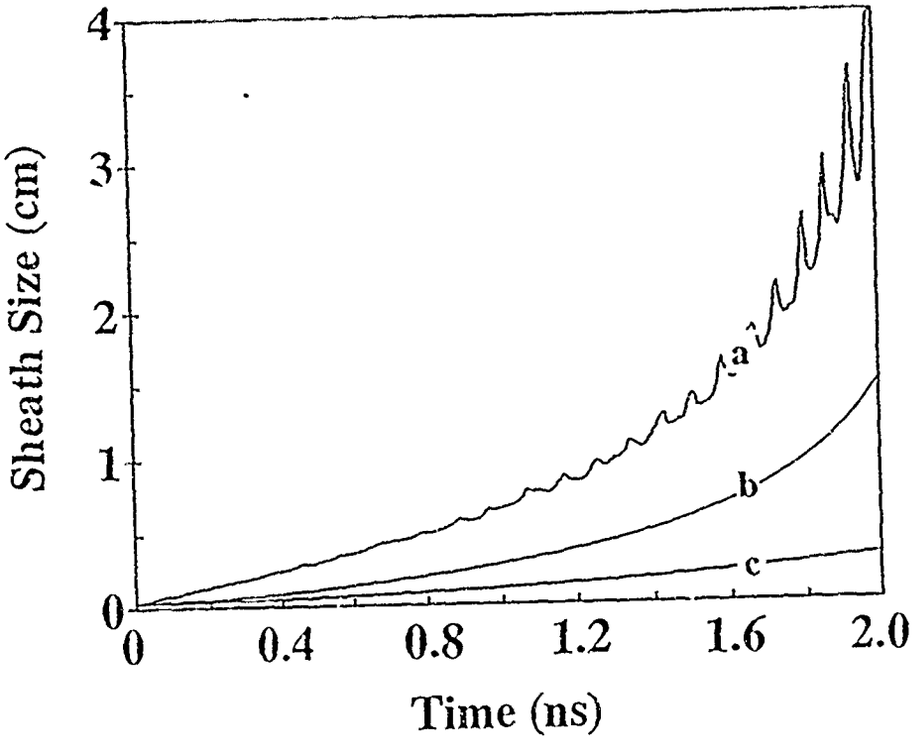

FIG. 12

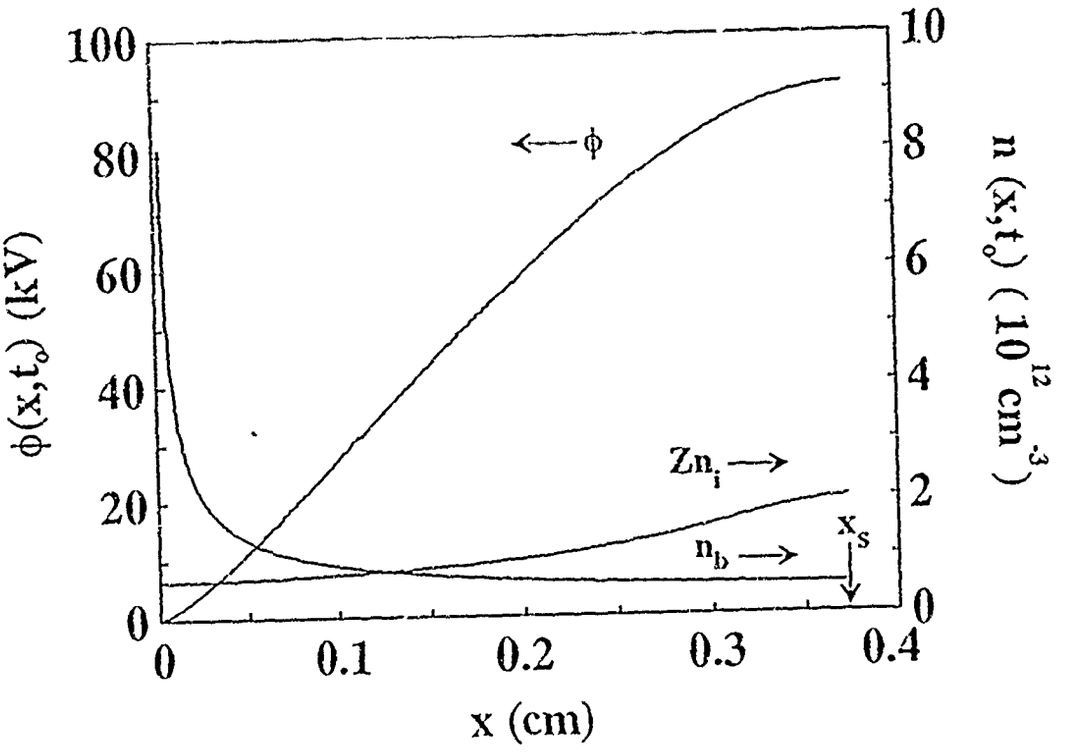
100
80
60
40
20
0
10
8
6
4
2
0
0
0.1
0.2
0.3
0.4
x (cm)
$\phi(x,t_o)$ (kV)
$n(x,t_o)$ (10^{12} cm^{-3})
$\leftarrow\phi$
$Zn_i \rightarrow$
$n_b \rightarrow$
x_s

FIG. 13

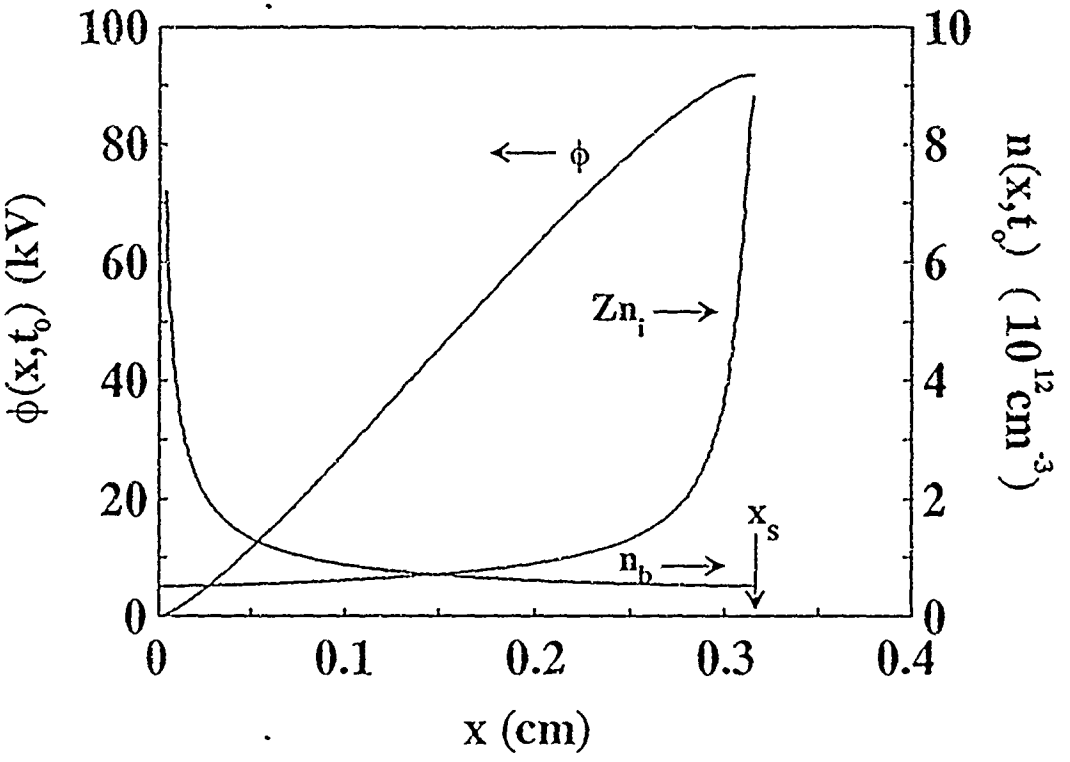
100
80
60
40
20
0
10
8
6
4
2
0
0
0.1
0.2
0.3
0.4
x (cm)
$\phi(x,t_o)$ (kV)
$n(x,t_o)$ (10^{12} cm^{-3})
$\leftarrow \phi$
$Zn_i \rightarrow$
$n_b \rightarrow$
x_s

FIG. 14

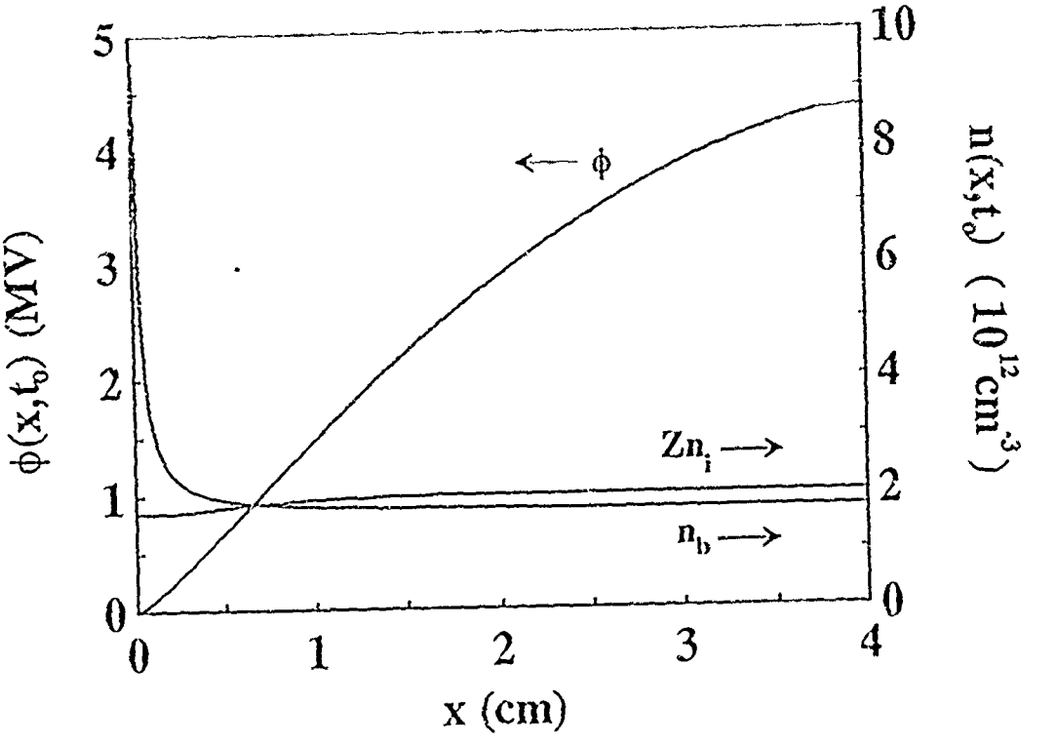
5
4
3
2
1
0
0
1
2
3
4
x (cm)
10
8
6
4
2
0
$\phi(x,t_0)$ (MV)
$n(x,t_0)$ ($10^{12}cm^{-3}$)
$\leftarrow \phi$
$Zn_i \rightarrow$
$n_b \rightarrow$

FIG. 15

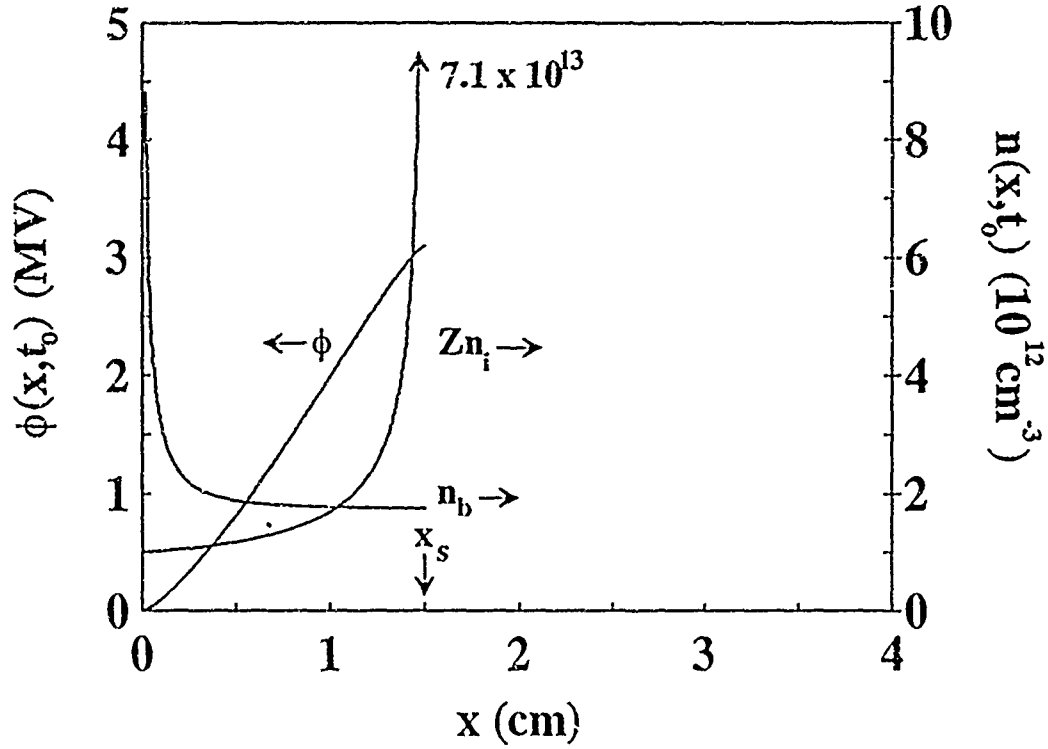
5
4
3
2
1
0
10
8
6
4
2
0
0
1
2
3
4
7.1 x 10^13
←φ
Zn_i→
n_b→
x_s
φ(x,t_o) (MV)
n(x,t_o) (10^12 cm^-3)
x (cm)

FIG. 16

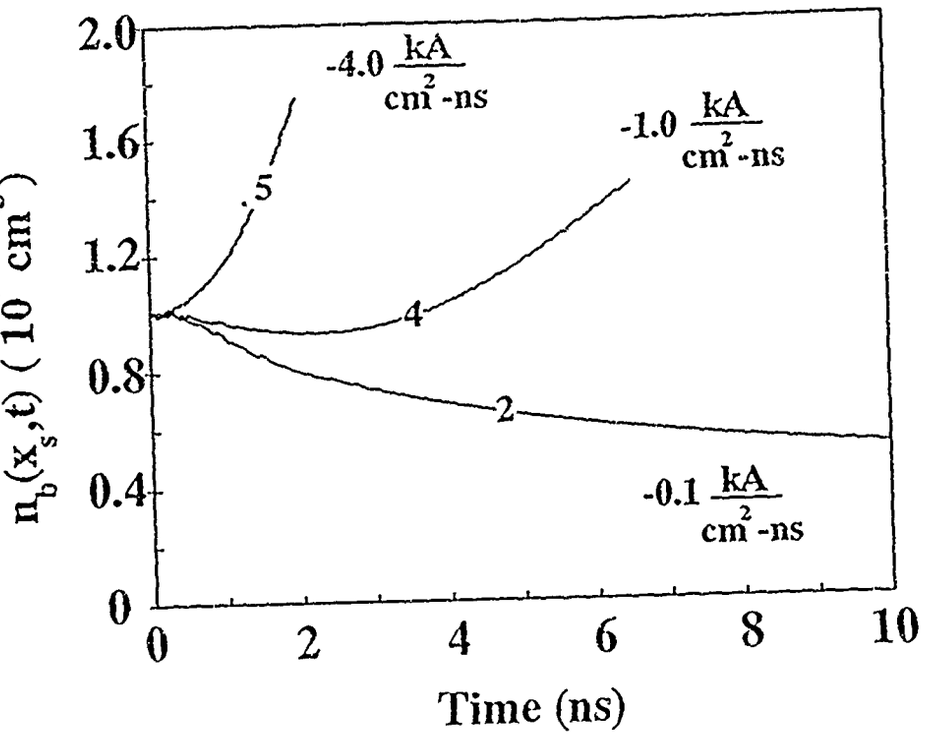
2.0
1.6
1.2
0.8
0.4
0
0
2
4
6
8
10
Time (ns)
$n_b(x_s,t)$ (10^{12} cm^{-3})
-4.0 kA / cm^2-ns
-1.0 kA / cm^2-ns
-0.1 kA / cm^2-ns
5
4
2

FIG. 17

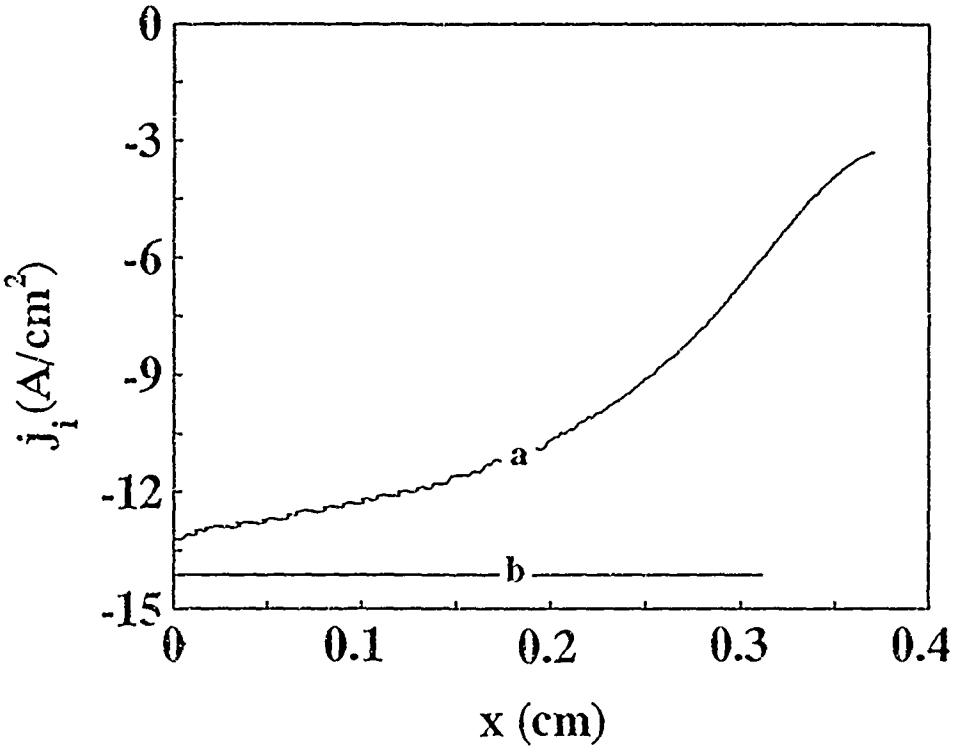

FIG. 18

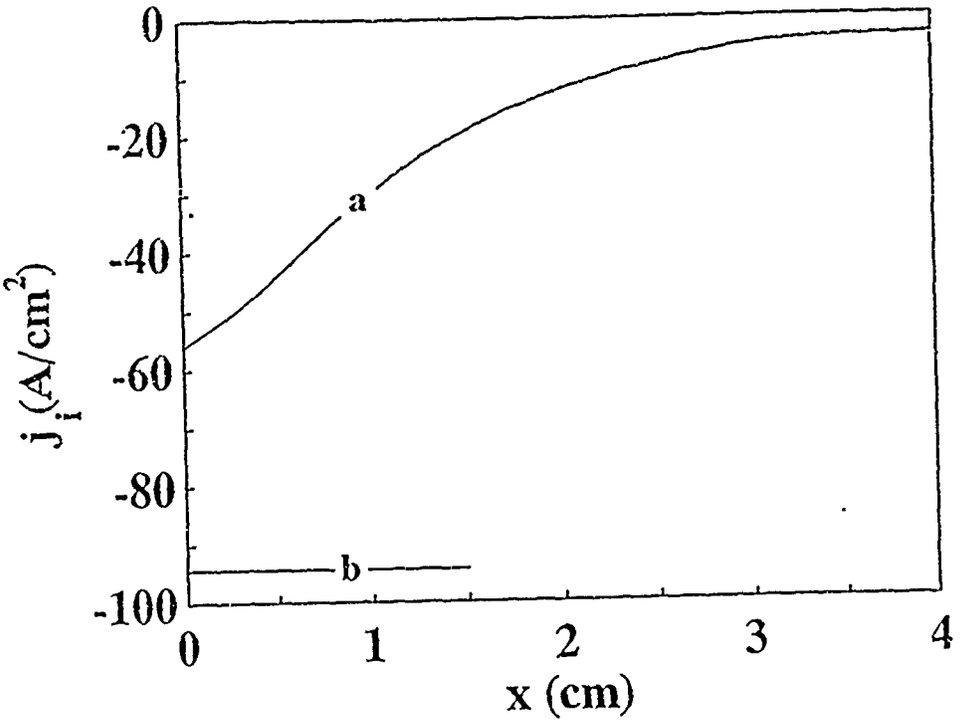

FIG. 19

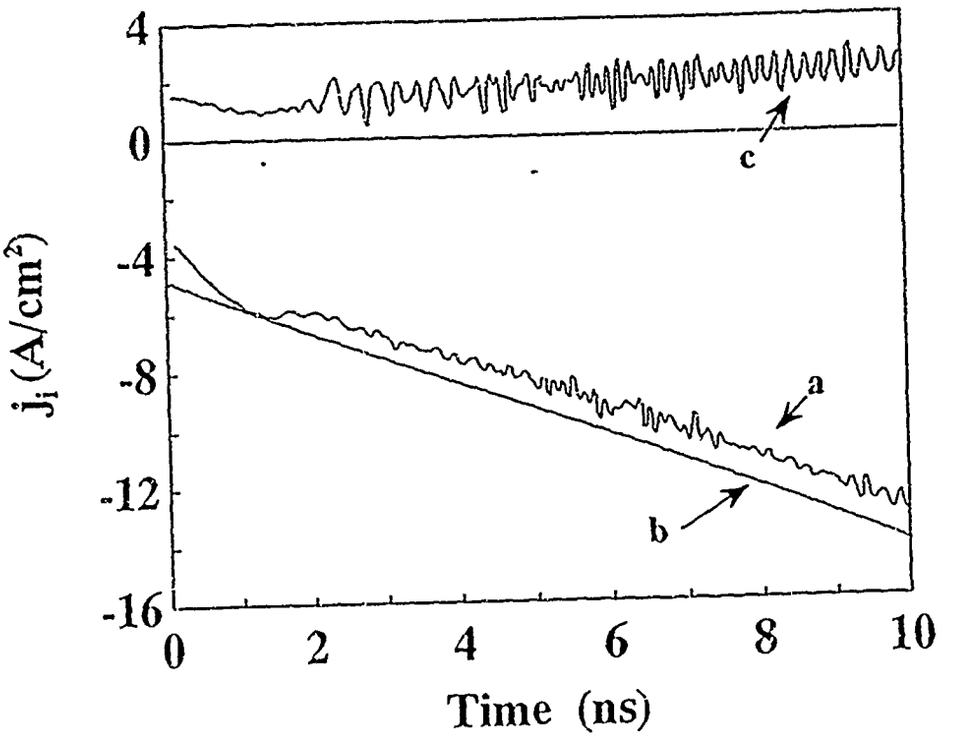

FIG. 20

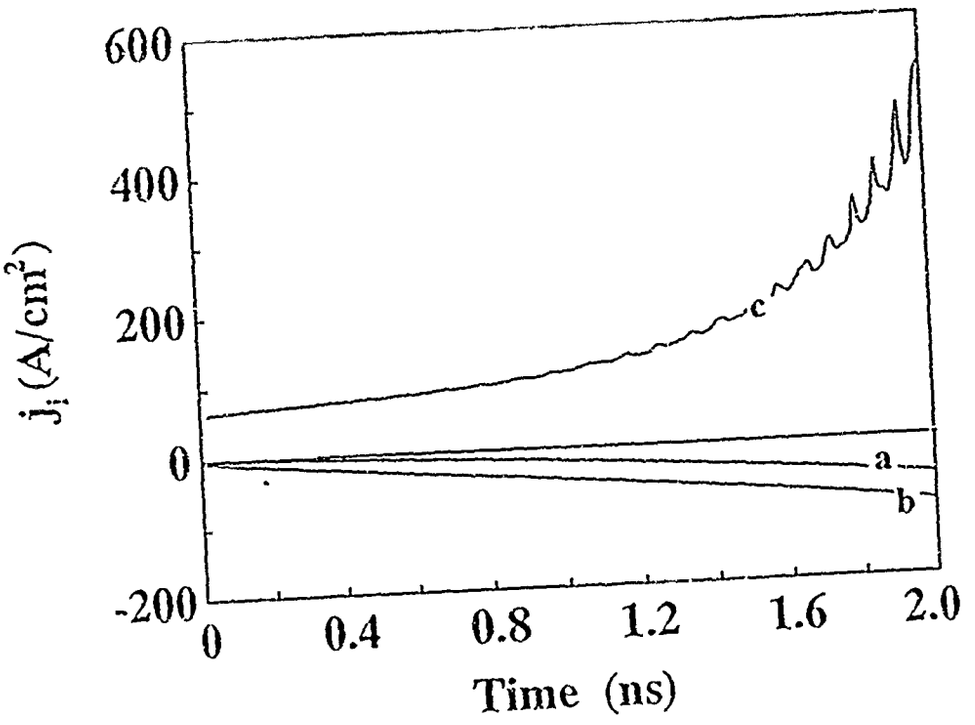

FIG. 21

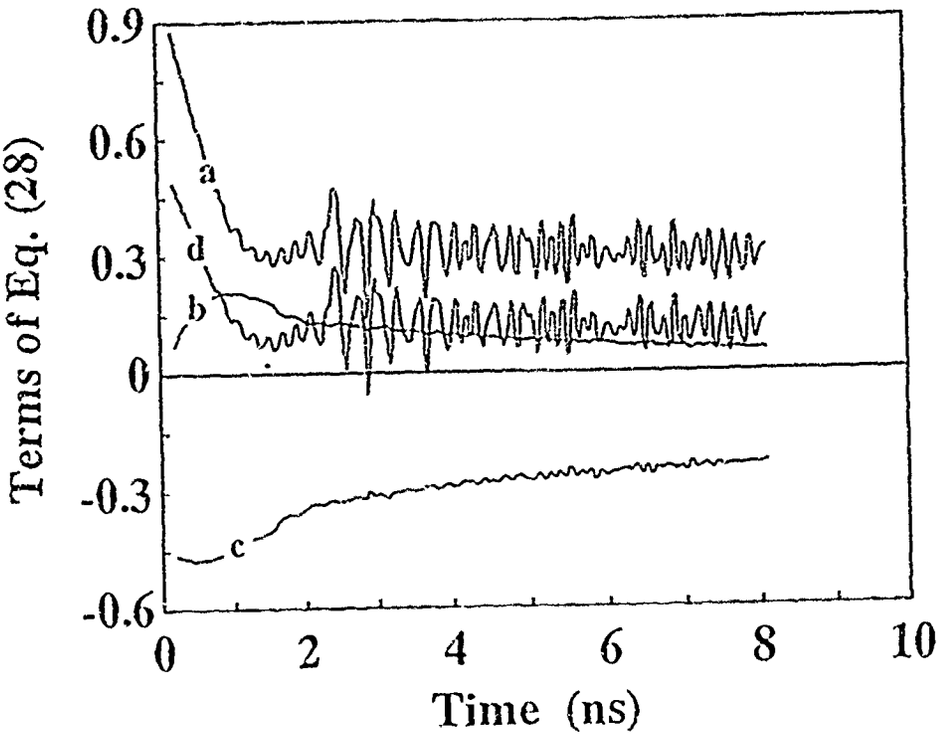

FIG. 22

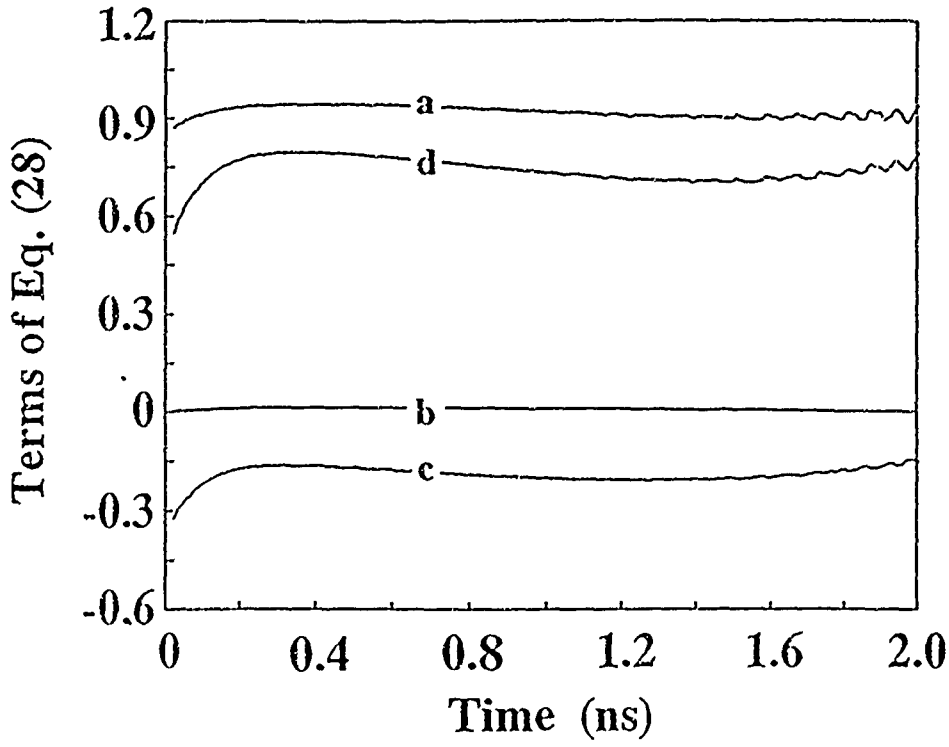

FIG. 23